

---

# Learning When to Act: Communication-Efficient Reinforcement Learning via Run-Time Assurance

---

Adam Haroon<sup>1,3\*</sup> Erick J. Rodríguez-Seda<sup>2</sup> Cody Fleming<sup>1</sup> Tristan Schuler<sup>3</sup>

<sup>1</sup>Department of Mechanical Engineering, Iowa State University, Ames, IA, USA

<sup>2</sup>Department of Weapons, Robotics, and Control Engineering,  
United States Naval Academy, Annapolis, MD, USA

<sup>3</sup>Navy Center for Applied Research in Artificial Intelligence (NCARAI),  
U.S. Naval Research Laboratory, Washington, D.C., USA

## Abstract

Safe reinforcement learning (RL) typically asks *what* an agent should do. We ask *when* it needs to act, and show that a single policy can jointly learn control inputs and communication-efficient timing decisions under a pointwise Lyapunov safety shield. We scope the framework to stabilization around a known equilibrium, where CARE-based LQR backups, Lyapunov certificates, and classical Lyapunov-STC are well defined, enabling a clean comparison against the analytical baseline. A run-time assurance (RTA) layer overrides the policy pointwise via a one-step-ahead Lyapunov prediction and a precomputed LQR backup, providing a strictly stronger guarantee than constrained MDP methods that enforce safety only in expectation. On an inverted pendulum, cart-pole, and planar quadrotor, the learned policy achieves  $1.91\times$ ,  $1.45\times$ , and  $3.51\times$  higher mean inter-sample interval (MSI) than a classical Lyapunov-triggered baseline; a fixed LQR controller at the same average rate is unstable on all three plants, showing that adaptive timing, not a lower average rate, is what makes sparsity safe. A CARE-derived Lyapunov reward transfers across environments without redesign, with a single weight  $w_c$  controlling the stability-communication tradeoff; ablations confirm the RTA shield is essential, with its removal reducing MSI by  $1.27\text{--}1.84\times$  and degrading state norms. A preference-conditioned extension recovers the full tradeoff frontier from a single model at  $\frac{2}{11}$  of training compute, and SAC experiments confirm the results are algorithm-agnostic across discrete and continuous domains. A 12-state 3D quadrotor case study extends the framework to higher-dimensional systems where classical STC design is analytically intractable: a SAC agent reaches  $\text{MSI} = 0.302\text{ s}$  (94% of  $\tau_{\max}$ ) at 0% RTA, while classical Lyapunov-STC remains pinned at  $\tau_{\min}$  and a fixed-rate LQR controller at the same average interval crashes within two control updates. Robustness to  $\pm 30\%$  plant-mass variation and additive disturbances confirms graceful degradation, with the RTA absorbing what the learned policy cannot.

## 1 Introduction

Safe reinforcement learning (RL) has made substantial progress on *what* an agent should do, but has largely ignored the question of *when* it needs to act. Fixed-rate control executes at every timestep regardless of whether the state has changed meaningfully; in safety-critical cyber-physical systems, this is expensive, consuming sensing, computation, and bandwidth on every update. Lifting this assumption without sacrificing safety is the central problem we address.

---

\*Corresponding author: aharoon@iastate.edu.

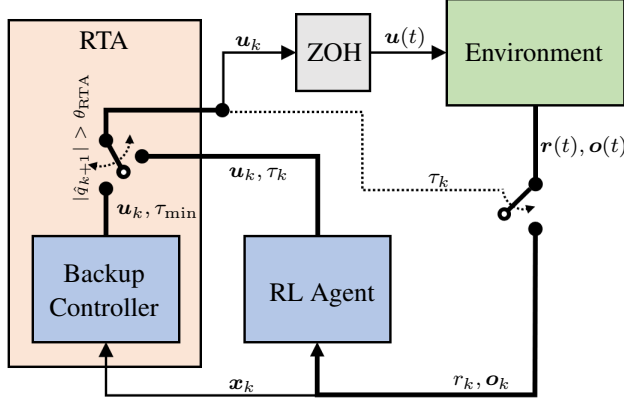


Figure 1: Proposed self-triggered control framework. The RL agent outputs a joint action  $(\mathbf{u}_k, \tau_k)$ . The RTA evaluates the one-step-ahead safety predicate  $|\hat{q}_{k+1}| > \theta_{\text{RTA}}$  on the linearized prediction of the next state and, if violated, substitutes the LQR backup at  $\tau_{\min}$ . The selected input is held by a zero-order hold (ZOH) until the next sampling instant  $t_k + \tau_k$ .

The control theory literature studies this as self-triggered control (STC) and event-triggered control (ETC) [16, 20, 6, 13, 30]: classical analytical methods determine the next update time from a Lyapunov or model-based triggering rule, providing strong stability guarantees but becoming difficult to apply to nonlinear, underactuated, or high-dimensional dynamics where the linearized one-step prediction leaves significant communication savings on the table. Learning-based approaches relax this conservatism by approaching the admissibility boundary empirically [7, 28, 11, 29, 3, 24, 27], but existing formulations either omit formal safety guarantees on the triggering decision [7, 28], rely on model-based learning of the dynamics [11], or address an interaction-cost continuous-time setting without a hard timing-safety mechanism [27]. Our framing differs on multiple axes: we operate in discrete-time STC where  $\tau_k$  is selected at each decision instant, with both discrete-action (DQN) and continuous-action (SAC) agents; we are model-free with a precomputed Linear-Quadratic Regulator (LQR) backup controller; and we provide *pointwise* Lyapunov-decreasing safety via a hard RTA override, a formal guarantee that expectation-level constraint methods such as Lagrangian-relaxation [5, 2] cannot provide by construction (Section 5.5).

We propose a unified RL framework (Fig. 1) that jointly selects the control input and the next inter-sample interval, supervised by an RTA layer acting as a safety shield [17, 19, 25]. The RTA uses a precomputed LQR backup and a one-step-ahead safety prediction to override unsafe actions, with each backup intervention provably unsaturated and Lyapunov-decreasing [4, 21, 10]. Episodes are time-bounded (not step-bounded), so a larger MSI directly reduces the number of agent decisions per episode of fixed duration: the operational quantity that communication efficiency targets. The RTA differs fundamentally from constrained MDP methods [5, 2, 14, 9, 12], which enforce safety only in expectation; we demonstrate empirically that a Lagrangian-DQN baseline using the identical constraint predicate achieves 21–52% lower MSI than RL-STC while accumulating up to 35% hard safety violations at the best checkpoint (Section 5.5). The framework is scoped to stabilization around a known equilibrium where CARE, Lyapunov analysis, and classical STC are well defined, enabling clean comparison; we evaluate on three lower-dimensional plants (inverted pendulum, CartPole, planar quadrotor) plus a 12-state 3D quadrotor case study (Section 6) where analytical STC design is intractable.

**Main contributions.** (1) A joint RL formulation that simultaneously learns control inputs and inter-sample intervals under a hard pointwise safety certificate (Proposition 1); unlike prior shielded RL that enforces safety at fixed time steps, our shield acts on the timing decision  $\tau_k$  itself. A single weight  $w_c$  traces the full stability/communication tradeoff frontier. (2) A CARE-derived Lyapunov reward that transfers across SISO and MIMO environments without redesign. (3) Systematic empirical validation on three lower-dimensional plants: 1.45–3.51  $\times$  MSI gains over Classical Lyapunov-STC, ablations isolating the RTA’s role, a Lagrangian-DQN comparison, a preference-conditioned extension at  $\frac{2}{11}$  compute, SAC confirming algorithm-agnosticism, and robustness under  $\pm 30\%$  mass variation and additive disturbances. (4) A 12-state 3D quadrotor case study showing the framework scales to higher-

dimensional MIMO systems where analytical STC design is intractable and where Proposition 1’s formal certificate does not extend at the chosen  $\tau_{\min}$ , testing the framework’s empirical reach beyond where the certificate applies (MSI = 0.302 s, 94% of  $\tau_{\max}$ , 0% RTA; Classical STC pinned at  $\tau_{\min}$ ; B2 unstable within two control updates).

## 2 Problem Formulation

### 2.1 Evaluation Scope

The framework targets stabilization around a known equilibrium. Three structural conditions are required for the safety certificates developed below: (i) a valid local linearization, (ii) a positive-definite quadratic Lyapunov function, and (iii) accuracy of the one-step-ahead prediction in (2). Stabilization around a known equilibrium guarantees all three: the linearization at the equilibrium is well posed, the CARE solution yields  $V(x) = x^\top Px$  that is positive-definite about that point, and the prediction is accurate within its neighborhood. Propositions 1 and 2 therefore hold under this scope.

### 2.2 Self-Triggered Control

Consider a continuous-time nonlinear plant  $\dot{x}(t) = f(x(t), u(t))$ , where  $x \in \mathbb{R}^n$  is the state and  $u \in \mathbb{R}^m$  is a piecewise-constant control input. In self-triggered control the controller executes at sampling instants  $\{t_0, t_1, \dots\}$  determined online. At each instant  $t_k$  the controller observes  $x_k \triangleq x(t_k)$ , selects  $u_k$  held constant over  $[t_k, t_{k+1})$ , and decides

$$t_{k+1} = t_k + \tau_k, \quad \tau_k \in \mathcal{T} = \{\tau_{\min}, 2\tau_{\min}, \dots, N\tau_{\min}\}, \quad (1)$$

where  $N$  is the cardinality of  $\mathcal{T}$ ; for consistency we choose  $N = 8$  across all experiments. The mean sampling interval (MSI) is the causal  $n$ -point moving average  $\text{MSI}_k = [(n-1)\text{MSI}_{k-1} + \tau_k]/n$ , initialized at  $\text{MSI}_0 = \tau_{\min}$ ; in what follows we take  $n = 5$ . A larger MSI corresponds to sparser communication; the objective is to maximize MSI subject to closed-loop stability. Episodes are time-bounded by a fixed simulation horizon  $T_{\max}$  rather than a fixed step count, so a larger MSI directly reduces the number of agent decisions per episode. This reflects what communication efficiency means in practice: fewer control updates per unit of operating time, and therefore lower demand on sensing, computation, and network bandwidth.

### 2.3 Run-Time Assurance

Run-time assurance augments the RL policy with a precomputed LQR backup (Section 3.1). At each step the linearized one-step-ahead prediction of the safety-critical scalar  $q_k = c^\top x_k$  is

$$\hat{q}_{k+1} = q_k + \tau_k \dot{q}_k + \frac{1}{2} \tau_k^2 \ddot{q}_{\text{lin}}(x_k, u_k). \quad (2)$$

If  $|\hat{q}_{k+1}| > \theta_{\text{RTA}}$  (or a position bound is exceeded), the RL action is overridden:

$$u_k \leftarrow \text{clip}_{\text{cw}}(-Kx_k, -u_{\max}, +u_{\max}), \quad \tau_k \leftarrow \tau_{\min}. \quad (3)$$

The threshold  $\theta_{\text{RTA}}$  is set strictly below the LQR saturation angle  $\theta_{\text{sat}} = u_{\max}/|K\theta|$  so that the backup retains full authority. The role of RL is not to guarantee safety, but to maximize performance within the safe set defined by the RTA layer, discovering non-conservative inter-sample intervals that would be difficult to obtain analytically.

**Proposition 1** (ZOH Lyapunov Decrease for the Linearized Backup). *Let*

$$M(\tau) \triangleq e^{A\tau} - \left( \int_0^\tau e^{As} ds \right) BK \quad (4)$$

*denote the ZOH-discretized closed-loop transition matrix that arises when the backup command  $u_k = -Kx_k$  is held constant on  $[t_k, t_k + \tau)$ , and suppose this command is component-wise unsaturated at  $x_k$  ( $|[-Kx_k]_i| < u_{\max,i}$  for all  $i$ ). Then  $x_{k+1} = M(\tau_{\min})x_k$  on the linearized plant, and  $V(x_{k+1}) \leq V(x_k)$  holds for all  $x_k$  if and only if*

$$M_{\text{disc}} \triangleq P - M(\tau_{\min})^\top P M(\tau_{\min}) \succeq 0.$$

Numerical verification (Table 4) confirms  $M_{\text{disc}} \succ 0$  for the Pendulum, CartPole, and planar Quadrotor environments. The Quadrotor3D plant fails this verification at its chosen  $\tau_{\text{min}}$ , retained deliberately for the case study (Section 6) which probes empirical behavior in the regime where the certificate does not extend.

Proof and an extended scope discussion are in Appendix A.

### 3 Method

#### 3.1 CARE-Based Lyapunov Function

For each environment we linearize the dynamics around the target equilibrium to obtain  $\dot{\mathbf{x}} = A\mathbf{x} + B\mathbf{u}$ . The Lyapunov function  $V(\mathbf{x}) = \mathbf{x}^\top P\mathbf{x}$  is obtained by solving the Continuous-time Algebraic Riccati Equation (CARE)

$$A^\top P + PA - PBR^{-1}B^\top P + Q = 0, \quad (5)$$

with  $Q \succ 0$ ,  $R \succ 0$ . The optimal LQR gain is  $K = R^{-1}B^\top P$  and the closed-loop matrix  $A_{\text{cl}} = A - BK$  is Hurwitz. By the CARE identity,  $\dot{V}(\mathbf{x}) \leq -\lambda V(\mathbf{x})$  along the linear closed-loop trajectory, where  $\lambda = \lambda_{\text{min}}(Q + K^\top RK, P)$  is the minimum generalized eigenvalue [8], yielding a tighter bound than the standard estimate. The Lyapunov value is normalized by  $V_{\text{scale}} = \text{tr}(P)/n$ .

**Proposition 2** (Admissible Inter-Sample Interval). *For the linear closed-loop system with  $P \succ 0$  solving (5), for any  $\mathbf{x}_k \neq \mathbf{0}$  there exists  $\tau^*(\mathbf{x}_k) > 0$  such that  $V(\mathbf{x}_{k+1}) < V(\mathbf{x}_k)$  for all  $\tau_k \in (0, \tau^*(\mathbf{x}_k))$ , where  $\mathbf{x}_{k+1} = M(\tau_k)\mathbf{x}_k$  is the ZOH solution under  $\mathbf{u}_k = -K\mathbf{x}_k$  with  $M(\cdot)$  from (4). On any compact annular region  $c \leq V(\mathbf{x}_k) \leq c'$ , a uniform constant  $\tau^+ > 0$  independent of  $\mathbf{x}_k$  exists with this property (Corollary A.3);  $\tau_{\text{min}}$  is verified numerically to satisfy  $\tau_{\text{min}} \leq \tau^+$  via  $M_{\text{disc}} \succ 0$  (Table 4).*

Proofs of Proposition 2 and Corollary A.3 are in Appendix A. Corollary A.4 (Appendix A) extends these results to the nonlinear plant with an explicit stability radius  $r^*$ .

#### 3.2 Action Space, Observations, and Reward

The agent selects a discrete action from a set of  $(\tau, \mathbf{u})$  tuples. For SISO environments  $\mathcal{A} = \mathcal{T} \times \mathcal{U}$ ; for the MIMO quadrotor  $\mathcal{A} = \mathcal{T} \times \mathcal{U}_{\delta F} \times \mathcal{U}_M$ . The agent observes  $\mathbf{o}_k = [\mathbf{x}_k^\top, \text{MSI}_k, b_k]^\top$ , where  $b_k \in \{0, 1\}$  flags whether the RTA was active on the previous step; including  $\text{MSI}_k$  enables credit assignment for the communication reward.

The per-step reward is

$$r_k = \underbrace{r_{\text{stab}} + 1 - \frac{V(\mathbf{x}_{k+1})}{V_{\text{scale}}}}_{\text{stability}} + \underbrace{w_c \left( \frac{\text{MSI}_k - \tau_{\text{min}}}{\tau_{\text{max}} - \tau_{\text{min}}} \right)^2}_{\text{communication}} + \underbrace{100 r_{\text{safe}}}_{\text{safety}}, \quad (6)$$

where  $r_{\text{stab}} = +1$  if  $V(\mathbf{x}_{k+1}) \leq V(\mathbf{x}_k)e^{-\lambda\tau_k}$  (with a near-origin guard  $V(\mathbf{x}_k) < \frac{1}{4}V_{\text{scale}}$  preventing penalization of residual oscillations) else  $-1$ ; the graded  $1 - V(\mathbf{x}_{k+1})/V_{\text{scale}}$  term provides a signal proportional to the absolute Lyapunov value;  $r_{\text{safe}} \in \{-1, 0\}$  flags RTA overrides; and a terminal penalty of  $-1000$  applies on constraint-violation termination. The weight  $w_c$  controls the stability/communication tradeoff; we sweep  $w_c \in \{0.25, 0.5, 1, 2, 4, 6, 8, 10, 12, 14, 16\}$ .

#### 3.3 DQN Training and Preference-Conditioned Extension

A DQN (256→128→128 ReLU) is trained for 1 M steps using Stable-Baselines3 [22] with best-model checkpointing at the per-step average-reward peak. Per-step rather than total-episode reward is the natural metric since episodes are time-bounded: a longer MSI yields fewer steps per fixed-duration episode. Per-step reward thus decouples policy quality from  $\tau_k$  choice. To avoid 11 separate per- $w_c$  sweeps, a *preference-conditioned DQN* [1, 31] samples  $w_c$  uniformly at each episode reset from the same grid and appends a log-normalized  $\hat{w}_c \in [0, 1]$  to the observation; at deployment  $w_c$  is fixed per-episode, so a single 2 M-step model recovers the per- $w_c$  frontier within 1–8% at  $\frac{2}{11}$  of total compute.

Table 1: Best-model checkpoint MSI (s) at the best-checkpoint peak  $w_c$  per algorithm. DQN values are 3-seed mean  $\pm$  std (Appendix E); SAC and Pref-DQN values are single-seed (seed 0). All three algorithms substantially exceed the Classical STC baseline and a fixed LQR at the same average rate is unstable on all three plants (B2, Table 2). Full per-weight sweep tables are in Appendix H.

Algorithm	Pendulum		CartPole		Quadrotor	
	MSI (s)	$w_c$	MSI (s)	$w_c$	MSI (s)	$w_c$
DQN	$0.397 \pm 0.001$	10	$0.308 \pm 0.014$	16	$0.281 \pm 0.018$	16
SAC	0.379	10	0.258	16	0.312	16
Pref-DQN (1 model)	0.393	16	0.316	14	0.266	16
Classical STC (B3)	0.202		0.212		0.080	

## 4 Environments

Four environments of increasing complexity span SISO and MIMO underactuated dynamics: the inverted pendulum (2 states, 1 input; Gymnasium Pendulum-v1), CartPole (4, 1; Gymnasium CartPole-v1 [26]), the planar quadrotor (6, 2; coupled MIMO hover with indirect horizontal control through tilt), and Quadrotor3D (12, 4; 6-DOF rigid-body quadrotor) used as the higher-dimensional case study. Each plant exhibits a distinct constraint geometry: the pendulum has the narrowest safety margin ( $\theta_{\text{sat}} - \theta_{\text{RTA}} = 1.9^\circ$ ); CartPole has a tight termination angle ( $12^\circ$ ) and large  $V_{\text{scale}} \approx 56.6$  that weakens the graded stability term; the planar quadrotor yields the largest MSI gain over Classical STC ( $3.51\times$ ) despite a  $9^\circ$  margin; Quadrotor3D’s 5,000-action discrete space rules out DQN, motivating SAC on the continuous Box action space, and is also deliberately chosen as a regime where Proposition 1’s formal certificate does not extend at the chosen  $\tau_{\text{min}}$ , enabling us to probe the framework’s empirical reach beyond where the certificate applies (Section 6). All integrate at  $\Delta t = 0.001$  s. Full dynamics, parameters (Table 5), and DQN/SAC hyperparameters are in Appendices B and C; compute resources and wall-clock times are in Appendix D.

## 5 Results

Each environment is trained for all 11  $w_c$  values; 100 deterministic evaluation episodes are run per checkpoint. We report MSI (mean  $\pm$  std), RTA activation rate (RTA%), and  $L_2$  state norms  $P_i = \sqrt{\int_0^T s_i^2(t) dt}$ . Full per-weight sweep tables for DQN, SAC, and Preference-Conditioned DQN appear in Appendix H.

### 5.1 DQN Results and Algorithm Comparison

Table 1 summarizes the best-model checkpoint MSI at the best-checkpoint peak  $w_c$  for each environment and algorithm. The DQN  $w_c$  sweeps and their corresponding ablation/Lagrangian comparisons are aggregated across 3 independent training seeds (Appendix E); all other rows use the standard single-seed protocol. The pendulum saturates near  $\tau_{\text{max}}$  from  $w_c = 6$  onwards. CartPole reaches 96% of  $\tau_{\text{max}}$  at  $w_c = 16$  with 0.04% RTA, despite a non-monotonic final-model trend caused by the large  $V_{\text{scale}}$  saturating the graded stability term. The quadrotor reaches 88% of  $\tau_{\text{max}}$ , reflecting the harder coupled hover dynamics. SAC achieves 0% RTA across every weight and environment in both the final model and best checkpoint, with no high- $w_c$  collapses, confirming that DQN collapses are a property of the discrete-action optimizer rather than the framework. The preference-conditioned DQN recovers the per- $w_c$  frontier within 1–8% from a single 2 M-step model, confirming that the full tradeoff frontier can be recovered at a fraction of total training compute.

**Off-policy methods are required in practice.** PPO [23] on the Pendulum either collapses to  $\tau_{\text{min}}$  or thrashes against the RTA shield at every  $w_c$  (best MSI  $\approx 0.09$  s vs. DQN’s  $0.397 \pm 0.001$  s); the rare-transition  $-100$  RTA and  $-1000$  terminal penalties are inherently easier for replay-based off-policy methods to leverage. The framework is algorithm-agnostic in principle, but practical convergence within standard training budgets favors off-policy methods (full sweep: Table 19, Appendix H).

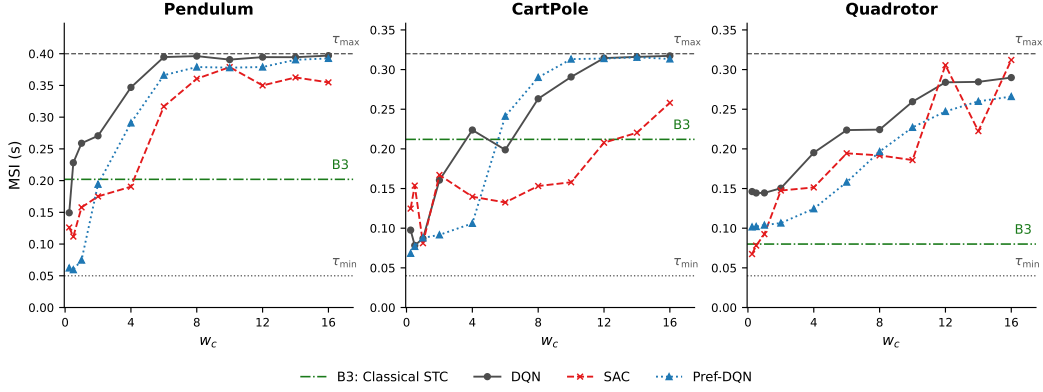


Figure 2: Best-model MSI vs.  $w_c$  for DQN, SAC, and Preference-Conditioned DQN across all three environments (seed-0 curves; multi-seed DQN aggregates are in Tables 10–12). Reference lines mark  $\tau_{\min}$  (dotted),  $\tau_{\max}$  (dashed), and Classical Lyapunov-STC baseline B3 (dash-dot green). All algorithms exceed B3 at moderate-to-high  $w_c$ ; the gap above B3 represents communication efficiency that conservative analytical methods leave on the table. DQN saturates near  $\tau_{\max}$  for Pendulum and CartPole; SAC converges more reliably but peaks slightly lower; Pref-DQN matches DQN within 1–8% from a single model.

## 5.2 Cross-Environment Analysis

Figure 2 summarizes the best-model MSI vs.  $w_c$ ; training dynamics (MSI, RTA activation, and episode reward curves) are in Appendix K (Fig. 4). Three patterns emerge across DQN, SAC, and Preference-Conditioned DQN. **(1)** Higher  $w_c$  accelerates MSI exploration: low- $w_c$  policies converge to  $\text{MSI} \approx \tau_{\min}$ ; high  $w_c$  pushes  $\tau_k$  toward  $\tau^*(\mathbf{x}_k)$  (Proposition 2), and all three methods exceed Classical Lyapunov-STC at moderate-to-high  $w_c$ . **(2)** At high  $w_c$  the optimizer overshoots admissibility, triggering sustained RTA intervention and reward degradation; the best-model checkpoint captures the MSI peak before this onset, with the canonical ablation  $w_c$  rising with complexity:  $w_c = 8$  for Pendulum (anchored within the saturation plateau,  $\geq 96\%$  of  $\tau_{\max}$ ) and  $w_c = 16$  for CartPole and Quadrotor (strict best-checkpoint peak). **(3)** Final-model degradation depends on plant geometry: Pendulum and Quadrotor tolerate high  $w_c$ , while CartPole’s large  $V_{\text{scale}} \approx 56.6$  and  $12^\circ$  termination margin produce non-monotonic final-model MSI; the best-model checkpoint is especially critical there, yielding a clean tradeoff ( $0.308 \pm 0.014$  s, 96% of  $\tau_{\max}$ ). Detailed per-environment analyses are in Appendix L.

## 5.3 Baseline Comparisons

Three baselines isolate the sources of communication efficiency ( $N_{\text{eval}} = 100$  each).

**B1 – Fixed LQR at  $\tau_{\min}$ :** Always stable, never communication-efficient. Establishes the hard safety floor.

**B2 – Fixed LQR at  $\tau_{\text{match}}$ :** The same LQR controller at a fixed interval equal to the seed-0 best-checkpoint MSI: 0.397 s (Pendulum), 0.317 s (CartPole), 0.290 s (Quadrotor). *This baseline is unstable on all three plants* (mean episode lengths 1.1–2.4 s), proving that adaptive timing, not merely a reduced average rate, is what makes sparsity safe: each plant’s unstable mode has a time constant shorter than  $\tau_{\text{match}}$  (e.g.,  $\sqrt{2l/(3g)} \approx 0.258$  s for the Pendulum’s rod dynamics), so the fixed-rate ZOH closed loop diverges. The RL policy avoids this by sampling fast near the unstable manifold and stretching  $\tau_k$  near equilibrium (Proposition 2).

**B3 – Classical Lyapunov-STC:** At each step the LQR control is applied and  $\tau_k$  is chosen greedily as the largest value in  $\mathcal{T}$  satisfying  $V(\tilde{\mathbf{x}}(\tau_k)) \leq V(\mathbf{x}_k)e^{-\lambda\tau_k}$ . This baseline maintains stability but achieves  $1.91\times$ ,  $1.45\times$ , and  $3.51\times$  lower MSI than RL-STC on Pendulum, CartPole, and Quadrotor respectively (Table 2); the gap is largest for the Quadrotor as the tight  $\hat{\theta}$  coupling pins the trigger near  $\tau_{\min}$ . The RL policy discovers that longer intervals are safe on average even where the instantaneous linearized Lyapunov bound is violated in the prediction.

Table 2: Baseline comparison ( $N_{\text{eval}} = 100$ ). RL-STC values are seed 0 to align with the  $\tau_{\text{match}}$  used for B2 (the seed-0 best-checkpoint MSI; multi-seed canonical bests differ by less than the  $\tau$ -grid spacing per Appendix F). *Italics* = system failure (ep. length  $< 3$  s); “-” = norms not meaningful for failed episodes.

Method	Pendulum			CartPole				Quadrotor					
	MSI	$P_3(\theta)$	$P_4(\dot{\theta})$	MSI	$P_1(x)$	$P_2(\dot{x})$	$P_3(\theta)$	$P_4(\dot{\theta})$	MSI	$P_1(x)$	$P_2(\dot{x})$	$P_3(\theta)$	$P_4(\dot{\theta})$
B1: LQR @ $\tau_{\text{min}}$	0.050	0.028	0.092	0.040	0.069	0.078	0.014	0.048	0.040	0.166	0.166	0.033	0.120
B2: LQR @ $\tau_{\text{match}}$	<i>0.397</i>	-	-	<i>0.317</i>	-	-	-	-	<i>0.290</i>	-	-	-	-
B3: Classical STC	0.202	0.026	0.167	0.212	0.065	0.094	0.013	0.097	0.080	0.160	0.164	0.034	0.349
<b>RL-STC</b>	<b>0.397</b>	0.605	0.916	<b>0.317</b>	1.637	2.361	0.325	2.105	<b>0.290</b>	2.640	1.916	0.463	5.664

Table 3: Ablation A – No RTA vs. full method ( $N_{\text{eval}} = 100$ , best-model checkpoint, 3 seeds per row; MSI as mean  $\pm$  std across the 3 per-seed mean values with ddof = 1,  $P_i$  norms as mean only;  $w_c = 8/16/16$  for Pendulum/CartPole/Quadrotor).

Method	Pendulum			CartPole				Quadrotor			
	MSI (s)	$P_3$	$P_4$	MSI (s)	$P_1$	$P_3$	$P_4$	MSI (s)	$P_1$	$P_3$	$P_4$
No RTA	0.266 $\pm$ 0.041	0.687	2.432	0.167 $\pm$ 0.042	5.813	0.428	5.036	0.222 $\pm$ 0.023	6.993	1.201	7.862
<b>RL-STC</b>	<b>0.385 <math>\pm</math> 0.014</b>	<b>0.636</b>	<b>1.049</b>	<b>0.308 <math>\pm</math> 0.014</b>	<b>2.955</b>	<b>0.401</b>	<b>2.796</b>	<b>0.281 <math>\pm</math> 0.018</b>	<b>2.334</b>	<b>0.523</b>	<b>5.171</b>

The RL-STC policy simultaneously achieves the high inter-sample sparsity of B2 *and* the full-episode stability of B1, demonstrating that the joint learning of control input and timing is necessary to unlock the communication efficiency that neither fixed-rate nor greedy trigger-based controllers can deliver. All reported  $P_i$  values correspond to episodes that completed the full 50 s horizon, confirming that larger excursions reflect higher-MSI trajectories rather than unstable operation.

#### 5.4 Ablation Study

**Ablation A – Removing the RTA Shield.** With the RTA override and penalty disabled ( $w_c = 8/16/16$ , canonical per Section 5.2), best-checkpoint MSI drops by  $1.27\text{--}1.84\times$  (Pendulum:  $0.385 \rightarrow 0.266$  s; CartPole:  $0.308 \rightarrow 0.167$  s; Quadrotor:  $0.281 \rightarrow 0.222$  s, Table 3), and state norms degrade substantially on CartPole and Quadrotor ( $P_1(x)$ :  $2.95 \rightarrow 5.81$  on CartPole,  $2.33 \rightarrow 6.99$  on Quadrotor;  $P_3(\theta)$  on Quadrotor degrades  $2.30\times$ ). The Lyapunov reward alone cannot replicate the RTA’s role: the shield shapes the feasible policy space during training and provides a hard safety floor at deployment that the learned policy can leverage.

Figure 3 provides geometric evidence: the RTA-enabled policy (top) occupies a compact high-reward region with  $1.27\text{--}1.84\times$  fewer control steps per episode (matching the inverse MSI ratios), while the no-RTA policy (bottom) visits a much wider region at substantially lower per-step rewards, isolating the RTA as a geometric constraint that enables long-interval strategies the Lyapunov reward alone cannot enforce.

**Ablation B – Fixed  $\tau$ .** Fixing  $\tau$  at the nearest grid value to  $\tau_{\text{match}}$  (with RTA active) and learning only the control input degenerates to LQR at  $\tau_{\text{min}}$  on Pendulum (RTA fires on 80.6% of steps), reaches a near-tie on CartPole only because  $\tau_{\text{match}} = \tau_{\text{max}}$  there, and gives up a 4.3% MSI advantage on Quadrotor. Joint optimization of  $(\mathbf{u}_k, \tau_k)$  is not separable; full results in Appendix F.

#### 5.5 Comparison with Lagrangian Safe RL

A Lagrangian-DQN baseline replaces the hard RTA override with a soft penalty  $r_k^{\text{Lag}} = r_k - \lambda_t c_k$  on the same one-step-ahead predicate ( $\lambda_t$  updated via dual gradient ascent). Across the three lower-dimensional environments, Lagrangian-DQN achieves 21–52% lower best-checkpoint MSI than RL-STC and accumulates up to 35.40% hard violations on Quadrotor, while RL-STC has zero hard violations by construction; final-model Lagrangian deteriorates further (e.g.,  $43.49 \pm 48.55\%$  hard violations on Pendulum, 59.35% on Quadrotor) as  $\lambda$  fails to hold the constraint across seeds. The hard override decouples safety from inter-sample interval selection during training, enabling long-interval commitment without the hedging that a soft penalty forces. Full per-environment results are in Appendix G, Table 9.

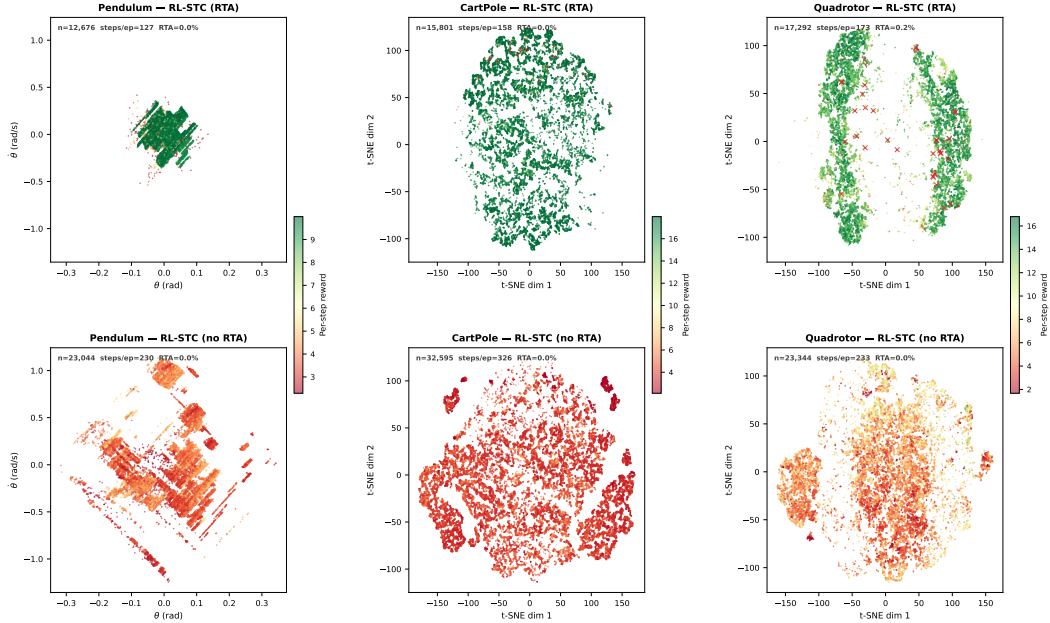


Figure 3: Per-step reward distribution (100 episodes; seed-0 trajectories per Appendix E): RL-STC (top) vs. no-RTA (bottom). Pendulum axes are  $(\theta, \dot{\theta})$ ; CartPole and Quadrotor use a shared t-SNE embedding fitted jointly on both policies’ trajectories. Color encodes per-step reward (green high, red low). The RTA-enabled policy occupies a compact high-reward region with  $1.27\text{--}1.84\times$  fewer steps per episode; the no-RTA policy visits a wider region at lower rewards.

## 5.6 Robustness

Best-model policies are evaluated under  $\pm 30\%$  mass mismatch and under additive constant, periodic, and impulse disturbances injected directly into the plant ( $K$ ,  $P$ , and RTA thresholds fixed at nominal). *Classical Lyapunov-STC fails on Pendulum and CartPole at  $0.7\times$  mass*, the faster actual dynamics exceeding the nominal prediction’s stability limit; RL-STC remains stable across all scales by trading MSI for safety. At  $0.7\times$  CartPole mass MSI drops 37% to 0.201 s with 13.91% RTA activation and recovers fully at  $1.3\times$ ; domain randomization over  $\pm 40\%$  mass eliminates the sensitivity at negligible cost to nominal performance. Under disturbances, RTA activation grows monotonically with amplitude while every episode completes safely (the filter absorbs what the policy cannot), and RL-STC maintains higher MSI than Classical STC under all conditions; the Quadrotor is structurally decoupled from thrust-channel disturbances, with MSI varying by at most 0.002 s across all conditions. Full mass-mismatch and disturbance tables (Appendix J, Tables 26 and 27) and per-channel analysis (Appendix M) are in the supplementary material.

## 6 Case Study: Scaling to Higher-Dimensional Systems

The three lower-dimensional environments share discrete action spaces of 168–792 actions that DQN can adequately cover. Quadrotor3D is qualitatively different: its 5,000-action discrete space leaves DQN with under 0.5 samples per action, rendering discrete learning intractable. We adopt SAC [15] on the equivalent continuous Box action space, keeping the reward, RTA, and Lyapunov construction identical. Training extends to 2 M steps with the policy widened to  $256\rightarrow 128\rightarrow 128$ , and the sweep extends to  $w_c \in \{0.25, 1, 4, 8, 16, 24, 32, 40, 48, 56, 64\}$ .

Pointwise safety in our framework decomposes into a *deployment-time* override and a *training-time* shaping signal (the RTA penalty cascading to the terminal penalty when the held backup propagates state out of bounds). The case study deliberately probes the regime where the deployment certificate does not extend: at  $\tau_{\min} = 0.04$  s the ZOH-discretized closed loop has spectral radius 1.19 ( $\tau_c \approx 0.037$  s), mirroring the conditions in which analytical STC design becomes intractable on higher-dimensional systems. The certificate could be restored locally by a smaller  $\tau_{\min}$  giving

$\tau_c > \tau_{\min}$ , a discrete-LQR redesign matched to  $\tau_{\min}$ , or a non-quadratic Lyapunov certificate; we instead test whether the training-time shaping alone produces a policy that respects the safety predicate. The trained policy maintains 0% RTA across the nominal sweep,  $\pm 30\%$  mass perturbation, and the disturbance suite reported below, a property of the trained policy on the tested distribution rather than a formal guarantee for states or conditions outside it.

**SAC sweep and Pref-SAC.** The sweep reveals a two-phase dynamic:  $w_c \leq 16$  keeps both final and best near  $\tau_{\min}$ ;  $w_c \geq 40$  saturates near  $\tau_{\max} = 0.32$  s at 0% RTA. We select  $w_c = 48$ , where the best-model checkpoint achieves  $\text{MSI} = 0.302$  s (94.3% of  $\tau_{\max}$ , 0% RTA) with low attitude norms ( $P_3(\varphi) \approx 0.04$ – $0.05$ ). A single preference-conditioned SAC model (4 M steps,  $w_c$  sampled per episode) reaches peak  $\text{MSI}$  0.239 s (79% of the per- $w_c$  SAC result) at  $\leq 0.01\%$  RTA across the full grid, recovering the frontier from one model.

**Baselines, ablations, and Lagrangian-SAC.** Classical Lyapunov-STC remains pinned at  $\tau_{\min}$  throughout: the one-step-ahead trigger is maximally conservative on the 12-state system, firing at every step. Baseline 2 (LQR at  $\tau_{\text{match}} = 0.302$  s) crashes in  $0.39 \pm 0.14$  s, fewer than two steps, the most dramatic confirmation that adaptive timing is a prerequisite. RL-STC achieves  $7.5\times$  longer inter-sample intervals than B1/B3 with attitude-rate norm  $P_4(p) = 0.190$  vs. 7.23. Removing the RTA (Ablation A) maintains  $\text{MSI} \approx 0.310$  s but roughly doubles attitude norms ( $P_3(\varphi)$ :  $0.044 \rightarrow 0.085$ ). Lagrangian-SAC converges to  $\text{MSI} \approx 0.311$ – $0.312$  s with zero hard violations, matching RL-STC empirically; SAC’s entropy regularization keeps the policy away from the constraint. Neither method holds a pointwise certificate on Q3D, but RL-STC retains a constructive path to Proposition 1 via discrete-LQR redesign or a smaller  $\tau_{\min}$  (Section 7), while Lagrangian-SAC admits no analytical extension.

**Robustness.** The nominal RL-STC policy shows *zero* degradation under  $\pm 30\%$  mass perturbation ( $\text{MSI}$  and RTA unchanged at 0.302 s and 0%), while Classical STC remains pinned at  $\tau_{\min}$  throughout. It also shows complete insensitivity to additive thrust disturbances (constant up to 1.0 N, periodic up to 1.5 N at 2 Hz, impulses up to 2.0 N):  $\text{MSI}$  remains 0.302 s with 0% RTA across all seven conditions, mirroring the structural decoupling in the 2D Quadrotor (the angular RTA trigger monitors tilt while thrust disturbances perturb the altitude channel). Full Q3D sweep, ablation, Lagrangian, mismatch, and disturbance tables are in Appendix I.

## 7 Limitations and Future Work

The RTA’s linearized one-step-ahead prediction grows conservative far from the operating point, the direct mechanism behind the empirical  $\text{MSI}$  ceiling and high- $w_c$  DQN collapses; a learned residual dynamics term could raise this ceiling without sacrificing the hard safety floor. The framework is scoped to stabilization around a known equilibrium so the CARE solution, quadratic  $V$ , and linearized one-step prediction remain well posed; non-equilibrium tasks (tracking, navigation, manipulation) and purely black-box dynamics lie outside this scope. Control barrier functions [14] offer a natural extension but require a different backup construction. Scaling beyond the 12-state Quadrotor3D to higher-dimensional systems, contact-rich dynamics, and real-world platforms remains the primary direction for future work.

## 8 Conclusion

We have presented a unified RL framework for communication-efficient self-triggered control with run-time assurance, evaluated across four environments from a 2-state pendulum to a 12-state 3D quadrotor case study. The CARE-derived Lyapunov reward transfers without redesign, and Proposition 2 provides a formal basis for the observed  $\text{MSI}$  ceiling. Three findings establish the framework’s value: **(i)** classical baselines fail (B2 unstable on all three lower-dimensional plants and crashes within two control updates on Quadrotor3D; B3 leaves a  $1.45$ – $3.51\times$   $\text{MSI}$  gap and remains pinned at  $\tau_{\min}$  on Quadrotor3D); **(ii)** on plants where  $M_{\text{disc}} \succeq 0$ , the RTA hard override delivers Lyapunov-decrease safety by construction regardless of algorithm, in contrast to Lagrangian-DQN which produces 21–52% lower  $\text{MSI}$  with up to 35% hard violations; **(iii)** ablations confirm RTA removal degrades  $\text{MSI}$  by 1.27–1.84 $\times$  and that joint optimization of  $(\mathbf{u}_k, \tau_k)$  is not separable. SAC and a preference-conditioned extension confirm algorithm-agnostic gains and frontier recovery at  $\frac{2}{11}$

of total compute. The Quadrotor3D case study reaches  $MSI = 0.302$  s (94% of  $\tau_{\max}$ ) with zero RTA activation, extending the framework to systems where analytical STC design is intractable and where the formal certificate does not extend at the chosen  $\tau_{\min}$ , and robustness experiments across all four plants confirm graceful degradation while every episode completes safely. The question of *when* to act is as consequential as *what* to do, and answering it safely and efficiently is tractable via the joint optimization this framework provides.

## Acknowledgments and Disclosure of Funding

A. Haroon conducted part of this work as an NREIP intern at the U.S. Naval Research Laboratory. The views expressed are those of the authors and do not reflect the official policy or position of the U.S. Naval Academy, Department of the Navy, Department of War, or U.S. Government.

## References

- [1] A. Abels, D. Roijers, T. Lenaerts, A. Nowé, and D. Steckelmacher. Dynamic weights in multi-objective deep reinforcement learning. In *International Conference on Machine Learning*, pages 11–20. PMLR, 2019.
- [2] J. Achiam, D. Held, A. Tamar, and P. Abbeel. Constrained policy optimization. In *International Conference on Machine Learning*, pages 22–31. PMLR, 2017.
- [3] S. Aggarwal, D. Maity, and T. Başar. Interq: A dqn framework for optimal intermittent control. *IEEE Control Systems Letters*, 2025.
- [4] M. Alshiekh, R. Bloem, R. Ehlers, B. Könighofer, S. Niekum, and U. Topcu. Safe reinforcement learning via shielding. In *Proceedings of the AAAI Conference on Artificial Intelligence*, volume 32, 2018.
- [5] E. Altman. *Constrained Markov Decision Processes*. Routledge, 2021.
- [6] A. Anta and P. Tabuada. To sample or not to sample: Self-triggered control for nonlinear systems. *IEEE Transactions on Automatic Control*, 55(9):2030–2042, 2010.
- [7] D. Baumann, J.-J. Zhu, G. Martius, and S. Trimpe. Deep reinforcement learning for event-triggered control. In *2018 IEEE Conference on Decision and Control (CDC)*, pages 943–950. IEEE, 2018.
- [8] S. Boyd, L. El Ghaoui, E. Feron, and V. Balakrishnan. *Linear Matrix Inequalities in System and Control Theory*. SIAM, 1994.
- [9] L. Brunke, M. Greeff, A. W. Hall, Z. Yuan, S. Zhou, J. Panerati, and A. P. Schoellig. Safe learning in robotics: From learning-based control to safe reinforcement learning. *Annual Review of Control, Robotics, and Autonomous Systems*, 5(1):411–444, 2022.
- [10] K. Dunlap, M. Mote, K. Delsing, and K. L. Hobbs. Run time assured reinforcement learning for safe satellite docking. *Journal of Aerospace Information Systems*, 20(1):25–36, 2023.
- [11] N. Funk, D. Baumann, V. Berenz, and S. Trimpe. Learning event-triggered control from data through joint optimization. *IFAC Journal of Systems and Control*, 16:100144, 2021.
- [12] J. Garcia and F. Fernández. A comprehensive survey on safe reinforcement learning. *Journal of Machine Learning Research*, 16(1):1437–1480, 2015.
- [13] T. Gommans, D. Antunes, T. Donkers, P. Tabuada, and M. Heemels. Self-triggered linear quadratic control. *Automatica*, 50(4):1279–1287, 2014.
- [14] S. Gu, L. Yang, Y. Du, G. Chen, F. Walter, J. Wang, and A. Knoll. A review of safe reinforcement learning: Methods, theories, and applications. *IEEE Transactions on Pattern Analysis and Machine Intelligence*, 46(12):11216–11235, 2024.

- [15] T. Haarnoja, A. Zhou, P. Abbeel, and S. Levine. Soft actor-critic: Off-policy maximum entropy deep reinforcement learning with a stochastic actor. In *International conference on machine learning*, pages 1861–1870. Pmlr, 2018.
- [16] W. P. Heemels, K. H. Johansson, and P. Tabuada. An introduction to event-triggered and self-triggered control. In *2012 IEEE 51st IEEE Conference on Decision and Control (CDC)*, pages 3270–3285. IEEE, 2012.
- [17] K. L. Hobbs, M. L. Mote, M. C. Abate, S. D. Coogan, and E. M. Feron. Runtime assurance for safety-critical systems: An introduction to safety filtering approaches for complex control systems. *IEEE Control Systems Magazine*, 43(2):28–65, 2023.
- [18] H. K. Khalil and J. W. Grizzle. *Nonlinear Systems*, volume 3. Prentice Hall Upper Saddle River, NJ, 2002.
- [19] C. Lazarus, J. G. Lopez, and M. J. Kochenderfer. Runtime safety assurance using reinforcement learning. In *2020 AIAA/IEEE 39th Digital Avionics Systems Conference (DASC)*, pages 1–9. IEEE, 2020.
- [20] M. Mazo and P. Tabuada. Decentralized event-triggered control over wireless sensor/actuator networks. *IEEE Transactions on Automatic Control*, 56(10):2456–2461, 2011.
- [21] K. Miller, C. K. Zeitler, W. Shen, K. Hobbs, J. Schierman, M. Viswanathan, and S. Mitra. Optimal runtime assurance via reinforcement learning. In *2024 ACM/IEEE 15th International Conference on Cyber-Physical Systems (ICCPs)*, pages 67–76. IEEE Computer Society, 2024.
- [22] A. Raffin, A. Hill, A. Gleave, A. Kanervisto, M. Ernestus, and N. Dormann. Stable-baselines3: Reliable reinforcement learning implementations, 2021.
- [23] J. Schulman, F. Wolski, P. Dhariwal, A. Radford, and O. Klimov. Proximal policy optimization algorithms. *arXiv preprint arXiv:1707.06347*, 2017.
- [24] L. Sedghi, Z. Ijaz, M. Noor-A-Rahim, K. Withephanich, and D. Pesch. Machine learning in event-triggered control: Recent advances and open issues. *IEEE Access*, 10:74671–74690, 2022.
- [25] D. Seto, B. Krogh, L. Sha, and A. Chutinan. The simplex architecture for safe online control system upgrades. In *Proceedings of the 1998 American Control Conference. ACC (IEEE Cat. No. 98CH36207)*, volume 6, pages 3504–3508. IEEE, 1998.
- [26] M. Towers, A. Kwiatkowski, J. Terry, J. U. Balis, G. De Cola, T. Deleu, M. Goulão, A. Kallinteris, M. Krimmel, A. KG, et al. Gymnasium: A standard interface for reinforcement learning environments. *arXiv preprint arXiv:2407.17032*, 2024.
- [27] L. Treven, B. Sukhija, Y. As, F. Dörfler, and A. Krause. When to sense and control? a time-adaptive approach for continuous-time rl. *Advances in Neural Information Processing Systems*, 37:63654–63685, 2024.
- [28] H. Wan, H. R. Karimi, X. Luan, and F. Liu. Model-free self-triggered control based on deep reinforcement learning for unknown nonlinear systems. *International Journal of Robust and Nonlinear Control*, 33(3):2238–2250, 2023.
- [29] R. Wang, I. Takeuchi, and K. Kashima. Deep reinforcement learning for continuous-time self-triggered control. *IFAC-PapersOnLine*, 54(14):203–208, 2021.
- [30] X. Wang and M. D. Lemmon. Event-triggering in distributed networked control systems. *IEEE Transactions on Automatic Control*, 56(3):586–601, 2010.
- [31] R. Yang, X. Sun, and K. Narasimhan. A generalized algorithm for multi-objective reinforcement learning and policy adaptation. *Advances in Neural Information Processing Systems*, 32, 2019.

## A Proofs

### A.1 Proof of Proposition 1

Under ZOH with  $\mathbf{u}_k = -K\mathbf{x}_k$  held constant on  $[t_k, t_k + \tau_{\min})$ , the linear plant  $\dot{\mathbf{x}} = A\mathbf{x} + B\mathbf{u}$  integrates to

$$\mathbf{x}(t_k + \tau_{\min}) = e^{A\tau_{\min}}\mathbf{x}_k + \left( \int_0^{\tau_{\min}} e^{As} ds \right) B \mathbf{u}_k = M(\tau_{\min})\mathbf{x}_k,$$

so  $\mathbf{x}_{k+1} = M(\tau_{\min})\mathbf{x}_k$ . Substituting into  $V(\mathbf{x}) = \mathbf{x}^\top P\mathbf{x}$  gives  $V(\mathbf{x}_{k+1}) = \mathbf{x}_k^\top M(\tau_{\min})^\top P M(\tau_{\min})\mathbf{x}_k$ , so  $V(\mathbf{x}_{k+1}) \leq V(\mathbf{x}_k)$  for all  $\mathbf{x}_k$  is equivalent to  $M_{\text{disc}} \succeq 0$ . Table 4 reports  $\lambda_{\min}(M_{\text{disc}}) > 0$  for the three lower-dimensional environments, directly verifying this condition.  $\square$

**Remark 1** (Scope of Proposition 1). *Proposition 1 certifies Lyapunov decrease in the  $P$ -weighted norm under the linearized ZOH closed loop with the held LQR backup, on the lower-dimensional environments where  $M_{\text{disc}} \succ 0$  holds. It is the discrete-time analog of  $A_{\text{cl}}$  being Hurwitz: each backup engagement weakly reduces the CARE-based Lyapunov certificate, driving the linearized closed loop toward the equilibrium. The proposition does not directly imply component-wise satisfaction of  $|q_{k+1}| < \theta_{\text{RTA}}$ , since decrease in the quadratic form  $V$  permits transient growth of individual state components. It also does not, on its own, certify Lyapunov decrease on the nonlinear plant under ZOH; Corollary A.4 provides a complementary nonlinear bound under continuous feedback within the conservative ball  $\mathcal{B}(r^*)$ . The choice  $\theta_{\text{RTA}} < \theta_{\text{sat}} = u_{\text{max}}/|K_\theta|$  ensures that, at engagement, the angle contribution to the backup satisfies  $|K_\theta q_k| < u_{\text{max}}$ ; together with the unsaturation hypothesis it provides the linear-ZOH grounding for the empirical pointwise safety observed across all evaluation conditions in Section 5. For Quadrotor3D,  $M_{\text{disc}} \succeq 0$  does not hold at the chosen  $\tau_{\min}$ , so this deployment-time certificate does not extend; the override remains active but uncertified, and the case study (Section 6) probes whether the training-time penalty cascade alone produces a policy that respects the safety predicate.*

### A.2 Proof of Proposition 2

Under ZOH with  $\mathbf{u}_k = -K\mathbf{x}_k$  held constant on  $[t_k, t_k + \tau)$ , the linear closed-loop solution is  $\mathbf{x}(\tau) = M(\tau)\mathbf{x}_k$  with  $M(\cdot)$  from (4). Define the Lyapunov difference  $\Delta V(\tau) \triangleq V(M(\tau)\mathbf{x}_k) - V(\mathbf{x}_k)$ ;  $M(0) = I$  gives  $\Delta V(0) = 0$ . Differentiating,

$$\frac{d}{d\tau}\Delta V(\tau) = \mathbf{x}_k^\top (\dot{M}(\tau)^\top P M(\tau) + M(\tau)^\top P \dot{M}(\tau)) \mathbf{x}_k.$$

Differentiating (4) gives  $\dot{M}(\tau) = Ae^{A\tau} - e^{A\tau}BK = e^{A\tau}(A - BK) = e^{A\tau}A_{\text{cl}}$ , so  $\dot{M}(0) = A_{\text{cl}}$ . Substituting at  $\tau = 0$  and applying the CARE identity  $A_{\text{cl}}^\top P + PA_{\text{cl}} = -(Q + K^\top RK) \prec 0$ ,

$$\left. \frac{d}{d\tau}\Delta V(\tau) \right|_{\tau=0} = \mathbf{x}_k^\top (A_{\text{cl}}^\top P + PA_{\text{cl}}) \mathbf{x}_k = -\mathbf{x}_k^\top (Q + K^\top RK) \mathbf{x}_k < 0$$

for all  $\mathbf{x}_k \neq \mathbf{0}$ . By continuity of  $\Delta V(\tau)$  in  $\tau$ , there exists  $\tau^*(\mathbf{x}_k) > 0$  such that  $\Delta V(\tau) < 0$  for all  $\tau \in (0, \tau^*(\mathbf{x}_k))$ .  $\square$

### A.3 Corollary A.3: State-Independent Admissible Interval

**Corollary 1.** *For any  $0 < c \leq c'$ , let  $\mathcal{A}_{c,c'} = \{\mathbf{x}_k : c \leq V(\mathbf{x}_k) \leq c'\}$ . There exists a constant  $\tau^+ > 0$ , independent of  $\mathbf{x}_k$ , such that  $\Delta V(\tau) < 0$  for all  $\tau \in (0, \tau^+)$  and all  $\mathbf{x}_k \in \mathcal{A}_{c,c'}$ . In particular,  $\tau_{\min}$  serves as such a  $\tau^+$ , verified numerically via  $M_{\text{disc}} \succ 0$  (Table 4).*

*Proof.* Let  $M_Q \triangleq Q + K^\top RK \succ 0$  (distinct from  $M(\tau)$  in Eq. (4)); from Proposition 2's derivative computation,  $d\Delta V/d\tau|_{\tau=0} = -\mathbf{x}_k^\top M_Q \mathbf{x}_k$ . On  $c \leq V(\mathbf{x}_k) \leq c'$ ,  $\|\mathbf{x}_k\|^2 \geq c/\lambda_{\max}(P)$ , so  $\mathbf{x}_k^\top M_Q \mathbf{x}_k \geq \lambda_{\min}(M_Q)c/\lambda_{\max}(P) > 0$  uniformly. Since  $\Delta V(0) = 0$  and  $d\Delta V/d\tau|_{\tau=0} \leq -\lambda_{\min}(M_Q)c/\lambda_{\max}(P) < 0$  uniformly, joint continuity of  $\Delta V(\tau, \mathbf{x}_k)$  implies the existence of a uniform  $\tau^+ > 0$ .  $\square$

**Remark 2.** Under continuous state feedback,  $A_{\text{cl}}$  Hurwitz implies  $V(e^{A_{\text{cl}}\tau} \mathbf{x}_k) \leq V(\mathbf{x}_k)e^{-\lambda\tau}$  for all  $\tau \geq 0$  [18], so  $\tau^*(\mathbf{x}_k) = \infty$ . Under ZOH on the nonlinear plant, the true trajectory deviates from the linearized prediction  $M(\tau)\mathbf{x}_k$  as  $\tau_k$  grows, eventually violating the Lyapunov decrease guarantee. B2 confirms this: the fixed-rate ZOH controller at  $\tau_{\text{match}}$  is unstable across all four plants, whereas the RL policy is stable because it adapts  $\tau_k$  to remain within the local admissible bound.

#### A.4 Corollary A.4: Nonlinear Admissible Region

**Corollary 2.** Let  $\delta(\mathbf{x}) = f(\mathbf{x}) - (A\mathbf{x} + B\mathbf{u}_k)$  denote the nonlinear residual. Since  $\delta(\mathbf{0}) = 0$  and  $\nabla\delta(\mathbf{0}) = 0$ , there exists  $L_\delta > 0$  such that  $\|\delta(\mathbf{x})\| \leq L_\delta\|\mathbf{x}\|^2$  near the origin. With  $M_Q \triangleq Q + K^\top RK \succ 0$  as in the proof of Corollary A.3, the true Lyapunov derivative satisfies

$$\dot{V}(\mathbf{x}) \leq -\lambda_{\min}(M_Q)\|\mathbf{x}\|^2 + 2\lambda_{\max}(P)L_\delta\|\mathbf{x}\|^3.$$

Hence  $\dot{V}(\mathbf{x}) < 0$  for all  $\mathbf{x} \neq \mathbf{0}$  with  $\|\mathbf{x}\| < r^* \triangleq \lambda_{\min}(M_Q)/[2\lambda_{\max}(P)L_\delta]$ . Within  $\mathcal{B}(r^*)$ , LaSalle’s invariance principle implies asymptotic stability of the origin.

*Proof.* Write  $\dot{\mathbf{x}} = A_{\text{cl}}\mathbf{x} + \delta(\mathbf{x})$ . Then  $\dot{V}(\mathbf{x}) = \mathbf{x}^\top (A_{\text{cl}}^\top P + PA_{\text{cl}})\mathbf{x} + 2\mathbf{x}^\top P\delta(\mathbf{x}) \leq -\mathbf{x}^\top M_Q\mathbf{x} + 2\|\mathbf{x}\|\lambda_{\max}(P)\|\delta(\mathbf{x})\|$ . Using  $\mathbf{x}^\top M_Q\mathbf{x} \geq \lambda_{\min}(M_Q)\|\mathbf{x}\|^2$  and  $\|\delta(\mathbf{x})\| \leq L_\delta\|\mathbf{x}\|^2$  yields the stated bound. Setting the right-hand side negative yields  $r^*$ .  $\square$

**Remark 3.** The small values of  $r^*$  for CartPole and Quadrotor ( $r^* = 0.009$ , Table 4) reflect the use of a global quadratic bound on  $\|\delta(\mathbf{x})\|$  rather than a tight local estimate. The actual region of attraction is substantially larger and is explored empirically under the RTA shield throughout training.

Table 4: Theoretical quantities per environment.  $M_Q \triangleq Q + K^\top RK$  is the CARE-quadratic matrix (distinct from the ZOH transition  $M(\tau)$  in Eq. (4)).  $r^*$  is a conservative lower bound on the true region of attraction (Corollary A.4). The margin  $\theta_{\text{sat}} - \theta_{\text{RTA}}$  keeps the angle channel of the backup unsaturated.  $\lambda_{\min}(M_{\text{disc}})$  is the minimum eigenvalue of  $M_{\text{disc}} = P - M(\tau_{\text{min}})^\top P M(\tau_{\text{min}})$ ; positivity verifies Proposition 1 numerically. “–” indicates that the ZOH-discretized backup at  $\tau_{\text{min}}$  is not Lyapunov-decreasing (see Section 6). Angles in degrees;  $r^*$  in  $\|\mathbf{x}\|$ .

Env.	$\lambda_{\min}(M_Q)$	$\lambda_{\max}(P)$	$L_\delta$	$r^*$	$\theta_{\text{RTA}}$	$\theta_{\text{sat}}$	$\lambda_{\min}(M_{\text{disc}})$
Pendulum	1.548	17.81	0.374	0.116	8.6°	10.5°	0.063
CartPole	1.087	216.6	0.289	0.009	12.0°	29.9°	0.040
Quadrotor	1.220	28.71	2.301	0.009	9.6°	12.0°	0.046
Quadrotor3D	1.000	25.42	0.684	0.029	10.1°	12.6°	–

## B Environment Details

All environments integrate the nonlinear plant at  $\Delta t = 0.001$  s.

Table 5: Environment parameters (ordered by complexity).

Parameter	Pendulum	CartPole	Quadrotor	Quadrotor3D
State dim. $n$	2	4	6	12
Input dim. $m$	1	1	2	4
$\tau_{\text{min}}$ (s)	0.05	0.04	0.04	0.04
$\tau_{\text{max}}$ (s)	0.40	0.32	0.32	0.32
$ \mathcal{A} $	168	328	792	5,000
$\theta_{\text{RTA}} / \theta_{\text{term}}$ (deg)	8.6 / 60	12.0 / 12	9.6 / 30	10.1 / 30
$\lambda$	$\approx 6.23$	$\approx 0.244$	$\approx 0.78$	$\approx 0.80$
$V_{\text{scale}}$	$\approx 8.99$	$\approx 56.6$	$\approx 5.71$	$\approx 5.05$

### B.1 Pendulum (Gymnasium Pendulum-v1 Physics)

State  $\mathbf{x} = [\theta, \dot{\theta}]^\top$ ,  $\theta = 0$  at upright equilibrium. Equation of motion:  $\ddot{\theta} = (3g/2l) \sin \theta + (3/ml^2)u$ ,  $m = 1 \text{ kg}$ ,  $l = 1 \text{ m}$ ,  $g = 10 \text{ m/s}^2$ ,  $|u| \leq 2 \text{ Nm}$ ,  $|\dot{\theta}| \leq 8 \text{ rad/s}$ . Linearization around  $\theta = 0$ :  $A = [0, 1; 15, 0]$ ,  $B = [0; 3]$ . Design matrices  $Q = \text{diag}(10, 1)$ ,  $R = 1$  yield  $K \approx [10.92, 2.88]$ ,  $\lambda \approx 6.23$ ,  $V_{\text{scale}} \approx 8.99$ . RTA threshold  $\theta_{\text{RTA}} = 0.15 \text{ rad}$  ( $\approx 8.6^\circ$ ), saturation angle  $\theta_{\text{sat}} \approx 10.5^\circ$ . Episodes terminate at  $|\theta| > 60^\circ$  or  $t \geq 50 \text{ s}$ . Initial conditions:  $\theta_0 \in [-0.1, 0.1] \text{ rad}$ ,  $\dot{\theta}_0 \in [-0.5, 0.5] \text{ rad/s}$ . Action set:  $|\mathcal{T}| = 8$ ,  $|\mathcal{U}| = 21$ ,  $|\mathcal{A}| = 168$ .

### B.2 CartPole (Gymnasium CartPole-v1 Physics)

State  $\mathbf{x} = [x, \dot{x}, \theta, \dot{\theta}]^\top$ . Equations of motion:

$$\ddot{\theta} = \frac{g \sin \theta - \cos \theta (F + m_p L \dot{\theta}^2 \sin \theta) / m_t}{L(4/3 - m_p \cos^2 \theta / m_t)}, \quad \ddot{x} = \frac{F + m_p L (\dot{\theta}^2 \sin \theta - \ddot{\theta} \cos \theta)}{m_t},$$

$m_c = 1.0 \text{ kg}$ ,  $m_p = 0.1 \text{ kg}$ ,  $m_t = 1.1 \text{ kg}$ ,  $L = 0.5 \text{ m}$ ,  $g = 9.8 \text{ m/s}^2$ ,  $|F| \leq 20 \text{ N}$ . Let  $d = L(4/3 - m_p/m_t)$ ; linearizing around  $\mathbf{x}^* = \mathbf{0}$ :

$$A = \begin{bmatrix} 0 & 1 & 0 & 0 \\ 0 & 0 & -m_p L g / (m_t d) & 0 \\ 0 & 0 & 0 & 1 \\ 0 & 0 & g/d & 0 \end{bmatrix}, \quad B = \begin{bmatrix} 0 \\ 1/m_t + m_p L / (m_t^2 d) \\ 0 \\ -1/(m_t d) \end{bmatrix}.$$

Design matrices  $Q = \text{diag}(6, 1, 11.5, 5)$ ,  $R = 1$ . Saturation angle  $\theta_{\text{sat}} \approx 29.9^\circ$ ; RTA threshold  $\theta_{\text{RTA}} = 12^\circ$ ; additional trigger  $|x_k| \geq 1.92 \text{ m}$ . Episodes terminate at  $|\theta| > 12^\circ$ ,  $|x| > 2.4 \text{ m}$ , or  $t \geq 50 \text{ s}$  [26]. Action set:  $|\mathcal{T}| = 8$ ,  $|\mathcal{U}| = 41$ ,  $|\mathcal{A}| = 328$ .

### B.3 Planar Quadrotor (Hover Stabilization)

State  $\mathbf{x} = [x, z, \theta, \dot{x}, \dot{z}, \dot{\theta}]^\top$ , inputs  $\mathbf{u} = [\delta F, M]^\top$  (thrust deviation, pitching moment):  $\ddot{x} = -(F/m) \sin \theta$ ,  $\ddot{z} = (F/m) \cos \theta - g$ ,  $\ddot{\theta} = M/I$ ,  $F = mg + \delta F$ ,  $m = 1 \text{ kg}$ ,  $I = 0.05 \text{ kg m}^2$ ,  $g = 9.81 \text{ m/s}^2$ ,  $|\delta F| \leq 5 \text{ N}$ ,  $|M| \leq 1 \text{ Nm}$ . Linearization around hover:

$$A = \begin{bmatrix} 0 & 0 & 0 & 1 & 0 & 0 \\ 0 & 0 & 0 & 0 & 1 & 0 \\ 0 & 0 & 0 & 0 & 0 & 1 \\ 0 & 0 & -g & 0 & 0 & 0 \\ 0 & 0 & 0 & 0 & 0 & 0 \\ 0 & 0 & 0 & 0 & 0 & 0 \end{bmatrix}, \quad B = \begin{bmatrix} 0 & 0 \\ 0 & 0 \\ 0 & 0 \\ 1/m & 0 \\ 0 & 1/I \end{bmatrix}.$$

Design matrices  $Q = \text{diag}(2, 2, 10, 1, 1, 5)$ ,  $R = \text{diag}(0.1, 5)$ . Moment saturation angle  $\theta_{\text{sat}} \approx 11.96^\circ$ ; RTA threshold  $\theta_{\text{RTA}} \approx 9.57^\circ$  (80% of  $\theta_{\text{sat}}$ ); additional trigger  $|x_k|, |z_k| \geq 2.0 \text{ m}$ . Episodes terminate at  $|\theta| > 30^\circ$ ,  $|x|$  or  $|z| > 2.5 \text{ m}$ , or  $t \geq 50 \text{ s}$ . Initial conditions:  $x_0, z_0 \in [-0.3, 0.3] \text{ m}$ ,  $\theta_0 \in [-0.1, 0.1] \text{ rad}$ ,  $\dot{x}_0, \dot{z}_0, \dot{\theta}_0 \in [-0.3, 0.3]$ . Action set:  $|\mathcal{T}| = 8$ ,  $|\mathcal{U}_{\delta F}| = 11$ ,  $|\mathcal{U}_M| = 9$ ,  $|\mathcal{A}| = 792$ .

### B.4 Quadrotor3D (6-DOF Hover Stabilization)

State  $\mathbf{x} = [p_x, p_y, p_z, \varphi, \theta, \psi, v_x, v_y, v_z, p, q, r]^\top \in \mathbb{R}^{12}$ , inputs  $\mathbf{u} = [\delta F, \tau_\varphi, \tau_\theta, \tau_\psi]^\top \in \mathbb{R}^4$ , where  $\delta F = F - mg$  is the thrust deviation from hover and  $(\tau_\varphi, \tau_\theta, \tau_\psi)$  are body-axis torques. The nonlinear equations of motion are the standard rigid-body model  $\dot{\mathbf{p}}_{\text{inert}} = R(\varphi, \theta, \psi) \mathbf{v}_{\text{body}}$ ,  $\dot{\Theta} = W(\varphi, \theta) \boldsymbol{\omega}_{\text{body}}$ ,  $\dot{\mathbf{v}}_{\text{body}} = R^\top \mathbf{g} + (F/m) \mathbf{e}_z - \boldsymbol{\omega} \times \mathbf{v}$ ,  $I \dot{\boldsymbol{\omega}} = \boldsymbol{\tau} - \boldsymbol{\omega} \times I \boldsymbol{\omega}$ , with  $R(\cdot)$  the body-to-inertial rotation matrix,  $W(\cdot)$  mapping body angular rates to Euler-angle rates, and  $I = \text{diag}(I_{xx}, I_{yy}, I_{zz})$ . Physical parameters:  $m = 1 \text{ kg}$ ,  $I_{xx} = I_{yy} = 0.02 \text{ kg m}^2$ ,  $I_{zz} = 0.04 \text{ kg m}^2$ ,  $g = 9.81 \text{ m/s}^2$ ; integrated with RK4 at  $dt = 0.001 \text{ s}$ . Actuator limits:  $|\delta F| \leq 5 \text{ N}$ ,  $|\tau_\varphi|, |\tau_\theta| \leq 1 \text{ Nm}$ ,  $|\tau_\psi| \leq 0.5 \text{ Nm}$ . Linearizing around hover gives an  $A$  matrix in which translational and rotational channels decouple, with horizontal positions controlled indirectly via tilt ( $\dot{v}_x \approx g\theta$ ,  $\dot{v}_y \approx -g\varphi$ ). Design matrices  $Q = \text{diag}(2, 2, 2, 10, 10, 1, 1, 1, 1, 5, 5, 1)$  and  $R = \text{diag}(0.1, 5, 5, 10)$  yield  $|K_{\tau_\varphi, \varphi}| \approx 4.55 \text{ Nm/rad}$ ,

giving  $\theta_{\text{sat}} \approx 12.60^\circ$  and the RTA threshold  $\theta_{\text{RTA}} \approx 10.08^\circ$  (80% of  $\theta_{\text{sat}}$ ); the one-step-ahead predicate is evaluated independently for  $\hat{\varphi}_{k+1}$  and  $\hat{\theta}_{k+1}$ . Additional trigger:  $|p_x|, |p_y|, |p_z| \geq 2.0$  m. Episodes terminate at  $|\varphi|$  or  $|\theta| > 30^\circ$ ,  $|\psi| > 90^\circ$ ,  $|p_x|, |p_y|, |p_z| > 2.5$  m, or  $t \geq 50$  s. Initial conditions:  $p_{x,0}, p_{y,0}, p_{z,0} \in [-0.3, 0.3]$  m,  $\varphi_0, \theta_0, \psi_0 \in [-0.1, 0.1]$  rad,  $v_{x,0}, v_{y,0}, v_{z,0} \in [-0.3, 0.3]$  m/s,  $p_0, q_0, r_0 \in [-0.1, 0.1]$  rad/s. Action set:  $|\mathcal{T}| = 8$ ,  $|\mathcal{U}_{\delta F}| = |\mathcal{U}_{\tau\varphi}| = |\mathcal{U}_{\tau\theta}| = |\mathcal{U}_{\tau\psi}| = 5$ , giving  $|\mathcal{A}| = 5,000$  for the discrete (DQN) variant; the SAC variant adopted in Section 6 uses the equivalent continuous Box action space.

## C Hyperparameters

Table 6: DQN hyperparameters (identical across all environments).

Hyperparameter	Value
Network architecture	256 $\rightarrow$ 128 $\rightarrow$ 128
Learning rate	$10^{-3}$
Replay buffer size	$10^6$
Batch size	64
Learning starts	64 steps
Discount factor $\gamma$	0.99
$\varepsilon$ -start / end	1.0 / 0.05
$\varepsilon$ decay steps	1,900
Total timesteps	1,000,000

Table 7: SAC hyperparameters (identical across all lower-dimensional environments; Quadrotor3D uses a wider 256 $\rightarrow$ 128 $\rightarrow$ 128 network and 2 M training steps as discussed in Section 6).

Hyperparameter	Value
Network architecture	128 $\rightarrow$ 64
Learning rate	$3 \times 10^{-4}$
Replay buffer size	$5 \times 10^5$
Batch size	128
Learning starts	1,000 steps
Discount factor $\gamma$	0.99
Soft update coefficient $\tau$	0.005
Entropy coefficient	automatic
Total timesteps	1,000,000

## D Compute Resources

DQN and SAC training budgets are reported in Tables 6 and 7: 1 M steps for DQN/SAC on the lower-dimensional environments, 2 M steps for preference-conditioned DQN, 2 M steps for SAC and PPO on Quadrotor3D, and 4 M steps for preference-conditioned SAC on Quadrotor3D. All experiments were run on a single workstation (Intel Core i9-13900KF, 24 cores / 32 threads; NVIDIA RTX 4090, 24 GB; 64 GB RAM; Ubuntu 22.04) via Stable-Baselines3. Wall-clock times for an 11-point  $w_c$  sweep run as 11 parallel processes are approximately 1 hour for the lower-dimensional DQN sweeps (1 M steps each), 6–7 hours for the lower-dimensional SAC sweeps (1 M steps each), and 13–15 hours for the Quadrotor3D SAC sweep (2 M steps each).

## E Multi-Seed Evaluation Methodology

For the lower-dimensional DQN  $w_c$  sweeps (Tables 10, 11, 12) and their corresponding No-RTA ablation (Table 3) and Lagrangian-DQN comparison (Table 9), we report results aggregated across the 3 independent training seeds  $\{0, 1, 2\}$ . Note that seed 0 is included in this set, so the seed-0 results referenced for single-seed experiments correspond to one of the three seeds in the multi-seed aggregates. For each seed we run the standard  $N_{\text{eval}} = 100$  deterministic evaluation; the per-seed

mean is the average over those 100 episodes. MSI and RTA-rate columns are then reported as the mean  $\pm$  standard deviation across the 3 per-seed mean values, using  $\text{ddof} = 1$  (unbiased estimator). The  $P_i$  state-norm columns report the mean across the 3 per-seed means only (no std), to keep the tables compact. All other experiments in the paper (SAC sweeps, Preference-Conditioned DQN, baselines, Ablation B, robustness studies, and the Quadrotor3D case study) use the standard single-seed evaluation protocol on **seed 0**, with std columns reflecting per-episode variance across the 100 evaluation episodes. Figures and tables that report RL-STC results without an explicit  $\pm$  across-seed annotation are accordingly seed-0 results unless labeled otherwise; we call this out per-table where relevant.

## F Ablation B: Fixed- $\tau$ Comparison

$\tau$  is fixed at the nearest grid value to  $\tau_{\text{match}}$  (the RL-STC best-checkpoint MSI for each environment); the agent optimizes only the control input. The RTA shield remains active.  $\tau_{\text{match}}$  is taken from the seed-0 best-checkpoint MSI, which sets the nearest grid value used for the fixed- $\tau$  comparison; seed 0 is one of the three seeds in the multi-seed evaluation (Appendix E), and its grid value is unchanged under multi-seed re-evaluation since the multi-seed mean differs from seed 0 by less than the grid spacing. The comparison below is reported on seed 0 throughout, keeping fixed- $\tau$  and RL-STC at the same seed.

For **Pendulum**, fixing  $\tau = 0.40$  s triggers RTA on 80.6% of steps, the shield resets  $\tau \leftarrow \tau_{\text{min}}$  on the majority of steps, degenerating the effective policy to LQR at  $\tau_{\text{min}}$  regardless of what the RL agent learns. This is the clearest demonstration that joint optimization of  $(\mathbf{u}_k, \tau_k)$  is not separable: it is precisely the learned adaptive inter-sample interval that allows the full policy to sustain an MSI of 0.396 s. For **CartPole**,  $\tau_{\text{match}} = \tau_{\text{max}}$ , so fixed- $\tau$  achieves essentially the same MSI as RL-STC (0.320 vs. 0.317 s) with no RTA, but this presupposes the stability/communication tradeoff point that RL-STC had to discover; for a plant where this does not coincide with  $\tau_{\text{max}}$ , RL-STC eliminates the search by incorporating interval selection into optimization. For **Quadrotor**, adaptive timing recovers a 4.3% MSI advantage (0.290 vs. 0.278 s) with lower  $P_1$ ; the higher  $P_4$  (5.664 vs. 4.342) reflects angular velocity excursion during higher-MSI hover corrections, not reduced stability.

Table 8: Ablation B: Fixed  $\tau$  vs. full method (best-model checkpoint,  $w_c = 8/16/16$ , seed 0).

Method	Pendulum ( $\tau_{\text{match}} = 0.40$ s)				CartPole ( $\tau_{\text{match}} = 0.32$ s)					Quadrotor ( $\tau_{\text{match}} = 0.28$ s)				
	MSI	RTA%	$P_3$	$P_4$	MSI	RTA%	$P_1$	$P_3$	$P_4$	MSI	RTA%	$P_1$	$P_3$	$P_4$
Fixed- $\tau$ RL	0.118	80.6	0.725	1.235	<b>0.320</b>	<b>0.0</b>	3.019	<b>0.330</b>	<b>2.523</b>	0.278	0.8	3.280	0.541	4.342
<b>RL-STC</b>	<b>0.396</b>	0.0	<b>0.271</b>	1.030	0.317	0.0	<b>2.879</b>	0.356	2.213	<b>0.290</b>	0.2	<b>2.640</b>	<b>0.463</b>	5.664

## G Lagrangian-DQN Detailed Results

The Lagrangian multiplier  $\lambda_t$  is updated via projected dual gradient ascent  $\lambda_{t+1} = \text{clip}(\lambda_t + \alpha_\lambda (g_t - \epsilon), 0, \lambda_{\text{max}})$  with budget  $\epsilon = 0.01$ ,  $\alpha_\lambda = 0.01$ . The critical difference from RL-STC is what happens when the predicate fires: RL-STC overrides the action so Hard Viol. = 0.0 by construction; Lagrangian-DQN applies only a soft penalty, so predicted events propagate into hard violations at rates that vary with plant complexity (Table 9). For **Pendulum**, Lagrangian achieves 21% lower MSI (0.304 vs. 0.385 s) with 7.95% hard violations, and the final model deteriorates to  $43.49 \pm 48.55\%$  hard violations as  $\lambda$  fails to hold across seeds. For **CartPole**, near-zero best-checkpoint hard violations come at 52% lower MSI (0.149 vs. 0.308 s); without a hard override, the policy must select shorter intervals to avoid violations, and final-model episodes terminate early at high rates, a failure invisible to the expectation-level constraint signal. For **Quadrotor**, 33% lower MSI (0.188 vs. 0.281 s) with 35.40% hard violations, deteriorating to 59.35% in the final model.

## H Full Sweep Tables

DQN sweeps (Tables 10–12) are 3-seed aggregates per Appendix E; all other sweeps in this section (SAC, Pref-DQN, PPO, and Quadrotor3D) are single-seed (seed 0), with  $\pm$  values in those tables reflecting per-episode variance across the 100 evaluation episodes.

Table 9: Lagrangian-DQN vs. RL-STC ( $N_{\text{eval}} = 100$ , 3 seeds per row;  $w_c = 8/16/16$  for Pendulum/CartPole/Quadrotor). MSI and the safety-event columns are reported as mean  $\pm$  std across the 3 per-seed mean values (ddof = 1). ‘‘Pred. Safety (%)’’ measures the same one-step-ahead predicate ( $|\hat{q}_{k+1}| > \theta_{\text{RTA}}$ ) for both methods: for RL-STC it is the RTA activation rate (predicate fires, action overridden, state violation prevented); for Lagrangian-DQN it is the constraint-violation rate (predicate fires, soft penalty only, no override). ‘‘Hard Viol. (%)’’ = fraction of executed timesteps where  $|\theta_k| > \theta_{\text{RTA}}$  in the actual trajectory. RL-STC Hard Viol. = 0.0 by construction of the pointwise override.

Method	Final Model			Best-Model Checkpoint		
	MSI (s)	Pred. Safety (%)	Hard Viol. (%)	MSI (s)	Pred. Safety (%)	Hard Viol. (%)
<i>Pendulum</i> ( $w_c = 8$ )						
Lagrangian-DQN	0.193 $\pm$ 0.080	41.95 $\pm$ 49.77	43.49 $\pm$ 48.55	0.304 $\pm$ 0.004	6.21 $\pm$ 4.02	7.95 $\pm$ 3.81
<b>RL-STC</b>	<b>0.343 <math>\pm</math> 0.039</b>	0.51 $\pm$ 0.84	<b>0.0</b>	<b>0.385 <math>\pm</math> 0.014</b>	0.37 $\pm$ 0.24	<b>0.0</b>
<i>CartPole</i> ( $w_c = 16$ )						
Lagrangian-DQN	0.121 $\pm$ 0.023	19.00 $\pm$ 29.81	0.26 $\pm$ 0.20	0.149 $\pm$ 0.033	0.48 $\pm$ 0.83	0.00 $\pm$ 0.00
<b>RL-STC</b>	<b>0.150 <math>\pm</math> 0.078</b>	11.61 $\pm$ 16.97	<b>0.0</b>	<b>0.308 <math>\pm</math> 0.014</b>	0.04 $\pm$ 0.06	<b>0.0</b>
<i>Quadrotor</i> ( $w_c = 16$ )						
Lagrangian-DQN	0.132 $\pm$ 0.020	65.65 $\pm$ 12.25	59.35 $\pm$ 12.54	0.188 $\pm$ 0.043	35.45 $\pm$ 5.76	35.40 $\pm$ 5.86
<b>RL-STC</b>	<b>0.151 <math>\pm</math> 0.057</b>	12.23 $\pm$ 14.25	<b>0.0</b>	<b>0.281 <math>\pm</math> 0.018</b>	1.96 $\pm$ 1.23	<b>0.0</b>

## H.1 DQN $w_c$ Sweep

Table 10: Pendulum – DQN  $w_c$  sweep ( $N_{\text{eval}} = 100$ , 3 seeds per row). MSI and RTA are reported as mean  $\pm$  std across the 3 per-seed mean values (ddof = 1);  $P_i$  norms are mean only. Bold marks the highest MSI in each section.

$w_c$	Final Model				Best-Model Checkpoint			
	MSI (s)	RTA (%)	$P_3(\theta)$	$P_4(\dot{\theta})$	MSI (s)	RTA (%)	$P_3(\theta)$	$P_4(\dot{\theta})$
0.25	0.185 $\pm$ 0.053	1.13 $\pm$ 1.94	0.660	2.521	0.214 $\pm$ 0.011	0.05 $\pm$ 0.04	0.448	2.303
0.5	0.105 $\pm$ 0.058	0.02 $\pm$ 0.03	0.803	1.786	0.234 $\pm$ 0.080	0.00 $\pm$ 0.00	0.312	1.403
1.0	0.246 $\pm$ 0.029	1.06 $\pm$ 1.68	0.637	2.292	0.252 $\pm$ 0.021	0.00 $\pm$ 0.01	0.396	1.510
2.0	0.261 $\pm$ 0.031	0.88 $\pm$ 1.40	0.564	2.636	0.293 $\pm$ 0.043	0.10 $\pm$ 0.17	0.384	1.669
4.0	0.209 $\pm$ 0.136	0.00 $\pm$ 0.01	0.369	1.180	0.358 $\pm$ 0.009	0.09 $\pm$ 0.15	0.274	1.135
6.0	0.249 $\pm$ 0.044	15.65 $\pm$ 25.32	0.563	2.710	0.385 $\pm$ 0.012	0.39 $\pm$ 0.34	0.575	1.182
8.0	0.343 $\pm$ 0.039	0.51 $\pm$ 0.84	0.564	2.091	0.385 $\pm$ 0.014	0.37 $\pm$ 0.24	0.636	1.049
<b>10.0</b>	<b>0.375 <math>\pm</math> 0.030</b>	<b>0.08 <math>\pm</math> 0.14</b>	0.534	1.443	0.397 $\pm$ 0.001	0.02 $\pm$ 0.03	0.434	1.028
12.0	0.355 $\pm$ 0.044	0.87 $\pm$ 1.40	0.581	1.428	0.392 $\pm$ 0.005	0.23 $\pm$ 0.31	0.615	1.114
14.0	0.363 $\pm$ 0.029	2.25 $\pm$ 3.57	0.556	2.022	0.378 $\pm$ 0.009	0.04 $\pm$ 0.05	0.497	1.460
<b>16.0</b>	0.306 $\pm$ 0.064	8.99 $\pm$ 15.53	0.515	2.138	<b>0.397 <math>\pm</math> 0.001</b>	<b>0.04 <math>\pm</math> 0.08</b>	0.415	1.017

## H.2 SAC $w_c$ Sweep

SAC achieves 0% RTA across every weight and environment in both the final model and best checkpoint, with no high- $w_c$  collapses. For the Quadrotor, the SAC best checkpoint at  $w_c = 16$  reaches 0.312 s versus DQN’s multi-seed best of  $0.281 \pm 0.018$  s, while maintaining 0% RTA. Across all three environments, the RTA shield and Lyapunov reward remain effective under a fundamentally different optimization algorithm, confirming that communication efficiency gains are a property of the framework, not of DQN.

## H.3 Preference-Conditioned DQN

The preference-conditioned DQN is trained once per environment for 2 M steps and evaluated at the same 11-point  $w_c$  sweep. For Pendulum, the best-model checkpoint achieves 0.393 s at  $w_c = 16$ , within 1% of standard DQN’s multi-seed best ( $0.397 \pm 0.001$  s) at  $\frac{2}{11}$  of compute. For CartPole, the best-model checkpoint plateaus near 0.313–0.316 s above  $w_c = 10$ , matching or slightly exceeding standard DQN ( $0.308 \pm 0.014$  s). For Quadrotor, the best checkpoint increases from 0.102 s to 0.266 s, within 5% of standard DQN ( $0.281 \pm 0.018$  s); the harder coupled hover dynamics remain challenging for a single shared policy at extreme  $w_c$ .

Table 11: CartPole – DQN  $w_c$  sweep ( $N_{\text{eval}} = 100$ , 3 seeds per row). MSI and RTA are reported as mean  $\pm$  std across the 3 per-seed mean values (ddof = 1);  $P_i$  norms are mean only. Bold marks the highest MSI in each section.

$w_c$	Final Model						Best-Model Checkpoint					
	MSI (s)	RTA (%)	$P_1(x)$	$P_2(\dot{x})$	$P_3(\theta)$	$P_4(\dot{\theta})$	MSI (s)	RTA (%)	$P_1(x)$	$P_2(\dot{x})$	$P_3(\theta)$	$P_4(\dot{\theta})$
0.25	0.124 $\pm$ 0.025	0.66 $\pm$ 0.54	1.35	3.88	0.380	4.834	0.146 $\pm$ 0.068	0.00 $\pm$ 0.00	2.79	3.09	0.350	3.716
0.5	0.105 $\pm$ 0.019	1.50 $\pm$ 1.30	1.87	4.45	0.410	5.570	0.136 $\pm$ 0.052	0.17 $\pm$ 0.29	3.79	3.94	0.394	5.019
1.0	0.099 $\pm$ 0.039	0.41 $\pm$ 0.25	3.07	3.34	0.367	3.958	0.130 $\pm$ 0.040	0.02 $\pm$ 0.03	2.63	4.51	0.403	5.959
2.0	0.117 $\pm$ 0.028	5.71 $\pm$ 7.03	2.23	4.12	0.395	4.898	0.142 $\pm$ 0.029	0.03 $\pm$ 0.03	2.58	3.83	0.466	4.416
4.0	0.135 $\pm$ 0.005	3.26 $\pm$ 1.47	2.76	3.87	0.361	4.647	0.191 $\pm$ 0.029	0.02 $\pm$ 0.02	2.26	4.74	0.474	5.810
6.0	0.148 $\pm$ 0.043	1.20 $\pm$ 1.65	3.25	4.12	0.363	5.088	0.231 $\pm$ 0.058	0.19 $\pm$ 0.30	4.38	4.25	0.428	4.765
8.0	0.155 $\pm$ 0.008	0.56 $\pm$ 0.70	4.56	3.86	0.432	4.665	0.282 $\pm$ 0.031	0.07 $\pm$ 0.13	2.55	3.12	0.401	3.214
10.0	<b>0.252 <math>\pm</math> 0.026</b>	<b>0.57 <math>\pm</math> 0.69</b>	1.94	3.62	0.407	3.949	0.294 $\pm$ 0.007	0.13 $\pm$ 0.14	2.66	3.19	0.385	3.369
12.0	0.152 $\pm$ 0.039	1.45 $\pm$ 0.89	1.74	4.36	0.372	5.414	0.302 $\pm$ 0.019	0.02 $\pm$ 0.03	2.43	3.69	0.398	4.058
14.0	0.189 $\pm$ 0.070	1.87 $\pm$ 1.80	4.59	5.11	0.440	6.299	0.293 $\pm$ 0.037	0.05 $\pm$ 0.09	2.54	3.29	0.400	3.435
<b>16.0</b>	0.150 $\pm$ 0.078	11.61 $\pm$ 16.97	3.72	3.60	0.322	3.964	<b>0.308 <math>\pm</math> 0.014</b>	<b>0.04 <math>\pm</math> 0.06</b>	2.95	3.27	0.401	2.796

Table 12: Quadrotor – DQN  $w_c$  sweep ( $N_{\text{eval}} = 100$ , 3 seeds per row). MSI and RTA are reported as mean  $\pm$  std across the 3 per-seed mean values (ddof = 1);  $P_i$  norms are mean only. Bold marks the highest MSI in each section.

$w_c$	Final Model						Best-Model Checkpoint					
	MSI (s)	RTA (%)	$P_1(x)$	$P_2(\dot{x})$	$P_3(\theta)$	$P_4(\dot{\theta})$	MSI (s)	RTA (%)	$P_1(x)$	$P_2(\dot{x})$	$P_3(\theta)$	$P_4(\dot{\theta})$
0.25	0.141 $\pm$ 0.013	1.12 $\pm$ 1.45	3.22	1.73	0.496	7.494	0.129 $\pm$ 0.053	0.05 $\pm$ 0.06	1.33	1.17	0.366	5.830
0.5	0.157 $\pm$ 0.019	1.62 $\pm$ 2.69	7.01	1.47	0.460	8.273	0.160 $\pm$ 0.027	0.54 $\pm$ 0.66	1.85	1.18	0.413	6.804
1.0	0.132 $\pm$ 0.009	1.69 $\pm$ 0.98	3.17	1.52	0.574	8.955	0.143 $\pm$ 0.043	0.02 $\pm$ 0.01	1.19	0.88	0.344	4.591
2.0	0.144 $\pm$ 0.053	0.44 $\pm$ 0.21	3.01	1.91	0.471	8.104	0.169 $\pm$ 0.039	0.39 $\pm$ 0.61	1.39	1.04	0.359	6.375
4.0	0.171 $\pm$ 0.023	1.96 $\pm$ 2.01	4.14	1.40	0.476	8.654	0.189 $\pm$ 0.029	0.27 $\pm$ 0.41	1.39	1.35	0.421	6.861
6.0	0.162 $\pm$ 0.020	0.50 $\pm$ 0.47	1.79	1.57	0.484	11.033	0.200 $\pm$ 0.023	0.38 $\pm$ 0.58	1.57	1.32	0.399	5.352
8.0	0.164 $\pm$ 0.040	1.00 $\pm$ 1.09	2.34	1.64	0.480	9.398	0.236 $\pm$ 0.025	0.54 $\pm$ 0.24	1.93	1.62	0.461	7.523
10.0	0.152 $\pm$ 0.041	0.80 $\pm$ 0.76	2.96	1.51	0.403	9.520	0.260 $\pm$ 0.016	0.69 $\pm$ 0.43	2.11	1.58	0.464	5.413
12.0	0.147 $\pm$ 0.049	7.02 $\pm$ 11.55	6.79	2.34	0.470	8.559	0.273 $\pm$ 0.010	0.42 $\pm$ 0.28	2.04	1.57	0.450	5.917
<b>14.0</b>	<b>0.203 <math>\pm</math> 0.008</b>	<b>0.40 <math>\pm</math> 0.40</b>	2.26	1.73	0.464	6.995	0.271 $\pm$ 0.018	1.14 $\pm$ 0.93	1.90	1.70	0.511	5.155
<b>16.0</b>	0.151 $\pm$ 0.057	12.23 $\pm$ 14.25	2.89	1.99	0.433	7.171	<b>0.281 <math>\pm</math> 0.018</b>	<b>1.96 <math>\pm</math> 1.23</b>	2.33	1.92	0.523	5.171

#### H.4 PPO $w_c$ Sweep (Pendulum)

Table 19 reports the full PPO sweep referenced from Section 5.1. No PPO checkpoint achieves communication efficiency comparable to DQN (0.396 s at  $w_c = 8$ ); runs that hold 0% RTA collapse to  $\tau_{\min} = 0.05$  s, while runs that explore longer intervals incur 45–80% RTA activation.

#### H.5 Quadrotor3D $w_c$ Sweeps

Tables 20 and 21 report the per- $w_c$  SAC sweep and the preference-conditioned SAC sweep on Quadrotor3D referenced from Section 6.

## I Quadrotor3D Ablations, Lagrangian Comparison, and Robustness

Tables 22 and 23 report the Quadrotor3D baseline/ablation comparison and the Lagrangian-SAC comparison referenced from Section 6; mass-mismatch and disturbance results are in Tables 24–25. All Q3D results are single-seed (seed 0) per Appendix E, with  $\pm$  values reflecting per-episode variance across the 100 evaluation episodes.

## J Robustness Tables

Tables 26 and 27 report the full model-mismatch and disturbance-robustness results. Detailed discussion of these results is in Appendix M.

## K Training Curves

Figure 4 shows DQN training curves (MSI, RTA activation rate, and per-step reward; see Section 3.3 for the per-step checkpoint rationale) for five  $w_c$  values across the three lower-dimensional environments. The MSI peak followed by reward collapse at high  $w_c$  directly motivates the best-model

Table 13: SAC – Pendulum  $w_c$  sweep ( $N_{\text{eval}} = 100$ , 1 M steps).

$w_c$	Final Model				Best-Model Checkpoint			
	MSI (s)	RTA (%)	$P_3(\theta)$	$P_4(\dot{\theta})$	MSI (s)	RTA (%)	$P_3(\theta)$	$P_4(\dot{\theta})$
0.25	0.0530 ± 0.0000	0.00	0.701	0.122	0.1261 ± 0.0008	0.00	0.164	0.098
0.5	0.0965 ± 0.0001	0.00	0.537	0.110	0.1118 ± 0.0455	0.00	0.689	0.240
1.0	0.0698 ± 0.0002	0.00	0.881	0.165	0.1578 ± 0.0028	0.00	0.106	1.646
2.0	0.1012 ± 0.0004	0.00	0.457	0.101	0.1751 ± 0.0046	0.00	0.233	1.312
4.0	0.0988 ± 0.0118	0.00	0.667	0.185	0.1904 ± 0.0315	0.00	0.370	0.162
6.0	0.3171 ± 0.0015	0.00	0.076	0.151	0.3168 ± 0.0016	0.00	0.046	0.145
8.0	0.3321 ± 0.0011	0.00	0.055	0.136	0.3605 ± 0.0014	0.00	0.051	0.141
<b>10.0</b>	<b>0.3656 ± 0.0018</b>	<b>0.00</b>	0.178	0.142	<b>0.3789 ± 0.0018</b>	<b>0.00</b>	0.134	0.146
12.0	0.3274 ± 0.0022	0.00	0.059	0.457	0.3500 ± 0.0022	0.00	0.064	0.271
14.0	0.3665 ± 0.0016	0.00	0.128	0.143	0.3626 ± 0.0017	0.00	0.134	0.144
16.0	0.3387 ± 0.0018	0.00	0.329	0.137	0.3548 ± 0.0018	0.00	0.340	0.141

Table 14: SAC – CartPole  $w_c$  sweep ( $N_{\text{eval}} = 100$ , 1 M steps).

$w_c$	Final Model						Best-Model Checkpoint					
	MSI	RTA (%)	$P_1$	$P_2$	$P_3$	$P_4$	MSI	RTA (%)	$P_1$	$P_2$	$P_3$	$P_4$
0.25	0.0663 ± 0.0000	0.00	5.215	0.597	0.065	0.208	0.1247 ± 0.0011	0.00	1.634	1.474	0.169	1.818
0.5	0.0651 ± 0.0000	0.00	0.975	0.127	0.018	0.084	0.1537 ± 0.0012	0.00	2.233	0.193	0.022	0.123
1.0	0.0801 ± 0.0001	0.00	1.582	0.220	0.029	0.188	0.0811 ± 0.0003	0.00	1.808	1.383	0.186	0.479
2.0	0.1104 ± 0.0119	0.00	2.200	0.200	0.020	0.062	0.1671 ± 0.0020	0.00	1.742	0.324	0.029	0.286
4.0	0.0569 ± 0.0000	0.00	3.715	0.787	0.124	0.506	0.1397 ± 0.0009	0.00	0.807	2.195	0.116	3.185
6.0	0.1067 ± 0.0002	0.00	2.374	1.624	0.260	0.906	0.1325 ± 0.0001	0.00	0.679	1.892	0.049	2.768
8.0	0.1617 ± 0.0002	0.00	3.041	0.571	0.040	0.681	0.1532 ± 0.0161	0.10	0.170	0.261	0.041	0.182
10.0	0.1476 ± 0.0001	0.00	1.344	0.210	0.026	0.131	0.1579 ± 0.0003	0.00	0.707	0.178	0.026	0.119
12.0	0.1978 ± 0.0006	0.00	0.280	0.134	0.018	0.067	0.2078 ± 0.0006	0.00	0.260	0.203	0.027	0.107
14.0	0.2037 ± 0.0004	0.00	0.833	0.197	0.027	0.102	0.2204 ± 0.0008	0.00	0.546	0.250	0.031	0.112
<b>16.0</b>	<b>0.2271 ± 0.0002</b>	<b>0.00</b>	2.758	0.228	0.025	0.112	<b>0.2581 ± 0.0003</b>	<b>0.00</b>	2.472	0.463	0.035	0.466

checkpoint strategy discussed in Section 5.2. SAC Quadrotor3D training curves are in Figure 5; SAC exhibits substantially smoother MSI and reward trajectories than DQN with no high- $w_c$  reward collapse, consistent with the algorithmic stability advantage that motivates the continuous-action variant for the higher-dimensional case study.

## L Detailed Per-Environment Analysis

### L.1 DQN: Per-Environment Discussion

**Pendulum.** The final-model MSI generally increases with  $w_c$ , peaking at  $w_c = 10$  ( $0.375 \pm 0.030$  s, 0.08% RTA), with the across-seed std reflecting training sensitivity at individual weights. The best-model checkpoint saturates near  $\tau_{\text{max}} = 0.40$  s from  $w_c = 6$  onwards with  $w_c \in \{10, 12, 16\}$  all achieving  $\text{MSI} \geq 0.39$  s and  $w_c = 16$  tying  $w_c = 10$  at the peak ( $0.397 \pm 0.001$  s). At the canonical  $w_c = 8$  used in ablations, the best checkpoint reaches  $0.385 \pm 0.014$  s ( $\geq 96\%$  of  $\tau_{\text{max}}$ ) with  $0.37 \pm 0.24\%$  RTA. The plateau is stable through  $w_c = 16$  with low RTA across seeds ( $\leq 0.5\%$  for  $w_c \geq 6$ ), demonstrating that pendulum dynamics fully saturate the sampling capacity of the  $\tau$  grid at moderate  $w_c$ .

**CartPole.** Two structural properties limit how high the final-model MSI can grow. First, CartPole’s CARE solution yields a large  $V_{\text{scale}} = 56.6$  (versus 8.99 for the Pendulum), because the  $\theta$  diagonal entry of  $P$  is approximately 196, a consequence of the high LQR cost of the indirect  $x$ -control path through  $\theta$ . Typical episode Lyapunov values are therefore a small fraction of  $V_{\text{scale}}$ , saturating the graded stability term  $1 - V(\mathbf{x}_{k+1})/V_{\text{scale}}$  near +1 throughout training, so the communication reward becomes the dominant differentiating signal even at low  $w_c$ . Second, the tight termination angle ( $\theta_{\text{term}} = 12^\circ$  vs.  $60^\circ$  for the Pendulum) means recovery from large inter-sample intervals carries higher penalty. Despite these constraints, the best-model checkpoint reveals a clean monotonic stability–communication tradeoff: MSI increases steadily from  $0.146 \pm 0.068$  s at  $w_c = 0.25$  to  $0.308 \pm 0.014$  s at  $w_c = 16$  with 0.04% RTA activity, 96% of  $\tau_{\text{max}}$ .

Table 15: SAC – Quadrotor  $w_c$  sweep ( $N_{\text{eval}} = 100$ , 1 M steps).

$w_c$	Final Model						Best-Model Checkpoint					
	MSI	RTA (%)	$P_1$	$P_2$	$P_3$	$P_4$	MSI	RTA (%)	$P_1$	$P_2$	$P_3$	$P_4$
0.25	0.0480 ± 0.0001	0.00	0.641	0.229	0.046	0.161	0.0674 ± 0.0029	0.00	0.260	0.194	0.048	0.176
0.5	0.0605 ± 0.0002	0.00	0.201	0.177	0.036	0.163	0.0781 ± 0.0006	0.00	0.193	0.173	0.035	0.156
1.0	0.0508 ± 0.0001	0.00	0.559	0.221	0.047	0.182	0.0925 ± 0.0013	0.00	0.416	0.500	0.096	0.254
2.0	0.0475 ± 0.0000	0.00	2.032	0.301	0.068	0.281	0.1475 ± 0.0021	0.00	0.479	0.144	0.038	0.168
4.0	0.1359 ± 0.0009	0.00	2.026	0.172	0.038	1.219	0.1514 ± 0.0015	0.00	1.899	0.260	0.096	2.382
6.0	0.1838 ± 0.0012	0.00	0.895	0.179	0.043	0.202	0.1944 ± 0.0014	0.00	0.211	0.180	0.044	0.224
8.0	0.1882 ± 0.0023	0.00	0.206	0.176	0.038	0.185	0.1918 ± 0.0023	0.00	0.201	0.167	0.038	0.240
10.0	0.1918 ± 0.0016	0.00	1.065	0.167	0.038	0.245	0.1859 ± 0.0019	0.00	0.669	0.165	0.038	0.207
12.0	0.3005 ± 0.0011	0.00	2.133	0.268	0.050	0.219	0.3055 ± 0.0021	0.00	2.056	0.302	0.051	0.188
14.0	0.2238 ± 0.0011	0.00	0.719	0.192	0.036	0.178	0.2224 ± 0.0013	0.00	0.985	0.225	0.043	2.304
16.0	<b>0.3100 ± 0.0008</b>	<b>0.00</b>	2.707	0.390	0.054	0.175	<b>0.3121 ± 0.0011</b>	<b>0.00</b>	2.973	0.378	0.062	0.395

Table 16: Preference-Conditioned DQN – Pendulum  $w_c$  sweep ( $N_{\text{eval}} = 100$ , 2 M steps, single model).

$w_c$	Final Model				Best-Model Checkpoint			
	MSI (s)	RTA (%)	$P_3$	$P_4$	MSI (s)	RTA (%)	$P_3$	$P_4$
0.25	0.1655 ± 0.0032	0.60	0.590	3.268	0.0623 ± 0.0014	0.00	0.352	0.797
0.5	0.1698 ± 0.0036	0.46	0.576	3.563	0.0596 ± 0.0016	0.00	0.347	0.777
1.0	0.1709 ± 0.0038	0.09	0.589	3.636	0.0747 ± 0.0044	0.42	0.475	2.525
2.0	0.1915 ± 0.0058	0.24	0.609	3.541	0.1943 ± 0.0098	0.52	0.601	3.580
4.0	0.2614 ± 0.0104	0.29	0.700	2.808	0.2909 ± 0.0082	0.54	0.531	3.180
6.0	0.3321 ± 0.0083	0.70	0.768	2.564	0.3661 ± 0.0064	0.92	0.408	2.107
8.0	0.3450 ± 0.0100	1.55	0.764	2.624	0.3790 ± 0.0083	1.98	0.445	2.320
10.0	0.3560 ± 0.0080	1.15	0.749	2.614	0.3780 ± 0.0122	4.10	0.436	2.199
12.0	0.3671 ± 0.0077	0.94	0.759	2.494	0.3790 ± 0.0201	3.95	0.432	2.165
14.0	0.3691 ± 0.0079	1.65	0.774	2.402	0.3904 ± 0.0167	1.33	0.366	1.976
16.0	<b>0.3705 ± 0.0088</b>	<b>1.58</b>	0.784	2.418	<b>0.3926 ± 0.0026</b>	<b>0.10</b>	0.350	1.798

**Quadrotor.** The final-model trend is intermediate between Pendulum and CartPole:  $w_c = 14$  yields the highest final-model MSI ( $0.203 \pm 0.008$  s, 0.40% RTA), while  $w_c = 16$  shows 12.23% RTA and  $w_c = 12$  shows 7.02% RTA as the policy overshoots the admissible inter-sample interval at the highest weights. The best-model checkpoint improves monotonically through the sweep, with  $w_c = 16$  achieving  $0.281 \pm 0.018$  s at 1.96% RTA, 88% of  $\tau_{\text{max}}$ , compared to 96% for Pendulum and CartPole, reflecting the harder coupled hover dynamics. The elevated  $P_4(\theta)$  values (3.6–12.6) across all weights are a structural property of the underactuated dynamics: to correct horizontal position error the policy must tilt the vehicle and return it to level, necessarily generating non-zero  $\dot{\theta}$  throughout the episode. This is not a sign of instability but an inherent consequence of the indirect coupling between  $M$  and  $x$ .

## L.2 SAC: Per-Environment Discussion

SAC reaches near-peak MSI for the Pendulum by  $w_c = 6$  and plateaus around 0.33–0.37 s, matching DQN’s best checkpoint with zero RTA everywhere. The DQN final model collapses at high  $w_c$ ; SAC’s final model remains stable, suggesting the continuous policy landscape is easier to optimize without collapsing into high-RTA regimes.

For CartPole, SAC eliminates the high-RTA collapses that plague DQN (38.6% at  $w_c = 0.5$ , 24.2% at  $w_c = 10$ ). All final models are stable and MSI increases monotonically with  $w_c$ , reaching 0.227 s at  $w_c = 16$ . The best checkpoint (0.258 s) falls short of DQN’s multi-seed best ( $0.308 \pm 0.014$  s), indicating that DQN transiently discovers sparser policies but cannot sustain them; SAC converges more reliably but has not yet matched DQN’s peak at 1 M steps.

For the Quadrotor, SAC matches DQN closely at moderate weights and surpasses it at high  $w_c$ : the SAC best checkpoint at  $w_c = 16$  reaches 0.312 s versus DQN’s  $0.281 \pm 0.018$  s, while maintaining 0% RTA. The final model also increases monotonically (0.310 s at  $w_c = 16$ ), in contrast to DQN’s 12.23% RTA at that weight. SAC’s stability advantage at high  $w_c$  further validates the benefit of continuous-action methods when DQN’s discrete policy degrades.

Table 17: Preference-Conditioned DQN – CartPole  $w_c$  sweep ( $N_{\text{eval}} = 100$ , 2 M steps, single model).

$w_c$	Final Model						Best-Model Checkpoint					
	MSI	RTA (%)	$P_1$	$P_2$	$P_3$	$P_4$	MSI	RTA (%)	$P_1$	$P_2$	$P_3$	$P_4$
0.25	0.1280 ± 0.0053	0.52	5.637	5.601	0.534	6.905	0.0683 ± 0.0112	1.08	2.060	3.014	0.353	3.609
0.5	0.1292 ± 0.0050	0.38	4.917	5.383	0.504	6.662	0.0770 ± 0.0109	2.71	1.511	2.388	0.270	2.867
1.0	0.1275 ± 0.0066	0.44	3.885	4.738	0.437	5.854	0.0878 ± 0.0094	5.99	1.536	2.524	0.267	3.060
2.0	0.1277 ± 0.0073	0.36	3.238	4.478	0.407	5.541	0.0916 ± 0.0111	6.66	1.894	2.636	0.271	3.185
4.0	0.1313 ± 0.0065	0.19	2.957	4.828	0.428	6.026	0.1061 ± 0.0141	6.38	2.213	2.518	0.260	3.032
6.0	0.1494 ± 0.0057	0.41	2.645	4.786	0.421	5.961	0.2412 ± 0.0260	1.34	3.104	3.174	0.311	3.779
8.0	0.1569 ± 0.0080	0.74	2.688	5.015	0.450	6.148	0.2901 ± 0.0070	0.00	2.404	3.467	0.368	3.874
10.0	0.1660 ± 0.0062	0.48	2.892	5.584	0.482	6.832	0.3132 ± 0.0021	0.00	2.882	3.206	0.366	3.272
12.0	0.1792 ± 0.0088	0.30	3.182	5.255	0.446	6.481	0.3139 ± 0.0028	0.02	2.421	2.992	0.350	2.990
14.0	0.1887 ± 0.0092	0.47	2.978	4.908	0.412	5.998	0.3155 ± 0.0028	0.04	2.645	3.017	0.364	2.885
<b>16.0</b>	<b>0.1892 ± 0.0106</b>	<b>0.77</b>	3.154	5.275	0.439	6.426	<b>0.3134 ± 0.0041</b>	<b>0.09</b>	2.562	2.969	0.366	2.809

Table 18: Preference-Conditioned DQN – Quadrotor  $w_c$  sweep ( $N_{\text{eval}} = 100$ , 2 M steps, single model).

$w_c$	Final Model						Best-Model Checkpoint					
	MSI	RTA (%)	$P_1$	$P_2$	$P_3$	$P_4$	MSI	RTA (%)	$P_1$	$P_2$	$P_3$	$P_4$
0.25	0.1115 ± 0.0075	0.13	8.029	1.573	0.368	6.173	0.1016 ± 0.0032	0.03	0.859	0.896	0.347	6.632
0.5	0.1067 ± 0.0077	0.35	7.171	1.782	0.400	6.500	0.1021 ± 0.0032	0.02	0.797	0.884	0.349	6.635
1.0	0.0937 ± 0.0053	0.46	5.622	2.150	0.391	6.003	0.1039 ± 0.0033	0.04	0.777	0.893	0.348	6.669
2.0	0.0689 ± 0.0019	0.08	2.757	1.336	0.222	3.309	0.1065 ± 0.0035	0.06	0.855	0.888	0.328	6.574
4.0	0.0645 ± 0.0007	0.01	8.756	0.763	0.157	2.337	0.1245 ± 0.0045	0.37	1.140	0.915	0.328	6.588
6.0	0.0990 ± 0.0062	0.13	3.692	1.501	0.335	5.197	0.1581 ± 0.0068	1.47	1.227	1.028	0.381	6.903
8.0	0.1530 ± 0.0078	1.04	3.706	1.868	0.396	7.268	0.1966 ± 0.0098	2.00	1.347	1.110	0.397	6.702
10.0	0.1641 ± 0.0088	10.99	11.162	1.925	0.520	6.724	0.2271 ± 0.0119	1.80	1.401	1.251	0.430	6.092
12.0	0.1493 ± 0.0097	11.45	11.773	1.958	0.536	6.740	0.2472 ± 0.0091	1.46	1.379	1.361	0.451	5.700
14.0	0.1420 ± 0.0096	14.63	11.694	2.135	0.566	6.878	0.2599 ± 0.0072	1.23	1.316	1.446	0.471	5.510
<b>16.0</b>	<b>0.1339 ± 0.0087</b>	<b>16.03</b>	<b>11.685</b>	<b>2.180</b>	<b>0.575</b>	<b>6.721</b>	<b>0.2660 ± 0.0066</b>	<b>1.42</b>	<b>1.401</b>	<b>1.518</b>	<b>0.488</b>	<b>5.388</b>

### L.3 Preference-Conditioned DQN: Per-Environment Discussion

For Pendulum, the preference-conditioned policy delivers a clean monotonic stability–communication tradeoff from a single 2 M-step training run. The final model reaches 0.371 s at  $w_c = 16$  with 1.6% RTA and exhibits no high- $w_c$  collapses, in contrast to the standard DQN final model. The best-model checkpoint achieves 0.393 s, matching the standard DQN best checkpoint (0.397 s) within 1% while using only  $\frac{2}{11}$  of the total training compute.

For CartPole, the preference-conditioned policy keeps RTA below 0.77% in the final model across all  $w_c$  values. The best-model checkpoint plateaus near 0.313–0.316 s above  $w_c = 10$ , matching or slightly exceeding the multi-seed standard DQN best ( $0.308 \pm 0.014$  s). A single 2 M-step run thus produces a clean monotonic tradeoff that matches the per- $w_c$  DQN ceiling at a fraction of the training compute.

For the Quadrotor, the best checkpoint increases monotonically from 0.102 s to 0.266 s, within 5% of multi-seed standard DQN ( $0.281 \pm 0.018$  s). The final model carries elevated RTA above  $w_c = 8$  (11–16%), indicating that the harder coupled hover dynamics remain challenging for a single shared policy at extreme communication weights. The best checkpoint maintains  $\leq 2\%$  RTA throughout the sweep, confirming that checkpoint selection is particularly important for the quadrotor at high  $w_c$ .

## M Detailed Robustness Analysis

### M.1 Model Mismatch: Detailed Discussion

**Pendulum degrades gracefully.** The Pendulum’s safety margin is only  $1.9^\circ$ . At  $0.7\times$  mass the pendulum swings faster for a given torque input, so the nominal one-step-ahead prediction systematically underestimates true angular velocity, causing RTA activation on  $30.48 \pm 24.80\%$  of steps. The large standard deviation (versus  $4.99 \pm 1.68\%$  at  $1.3\times$ ) indicates bimodal behavior: episodes that begin near the upright position are handled safely, while those with larger initial angles trigger persistent RTA engagement. Crucially, the system remains stable in all 100 episodes: the shield forces  $\tau_k \leftarrow \tau_{\min}$  on affected steps, cutting achieved MSI to 0.246 s but preventing divergence. At  $1.3\times$  mass the slower dynamics increase the margin available to the nominal prediction, reducing RTA to 4.99% and recovering most of the MSI (0.349 s vs. 0.396 s nominal).

Table 19: PPO – Pendulum  $w_c$  sweep ( $N_{\text{eval}} = 100$ , 2 M steps). Bold marks the highest MSI in each section.

$w_c$	Final Model				Best-Model Checkpoint			
	MSI (s)	RTA (%)	$P_3(\theta)$	$P_4(\dot{\theta})$	MSI (s)	RTA (%)	$P_3(\theta)$	$P_4(\dot{\theta})$
0.25	0.0633 ± 0.0028	45.02	0.479	1.412	0.0504 ± 0.0017	71.24	0.982	1.191
0.5	0.0873 ± 0.0033	10.08	0.541	1.289	0.0635 ± 0.0033	4.60	0.686	0.969
1.0	0.0885 ± 0.0075	30.72	0.336	0.924	0.0771 ± 0.0078	29.85	0.564	1.012
2.0	0.0500 ± 0.0000	0.00	0.169	1.001	0.0500 ± 0.0000	0.00	0.102	0.998
4.0	0.0639 ± 0.0006	0.00	0.044	0.626	0.0500 ± 0.0000	0.00	0.082	0.993
<b>6.0</b>	<b>0.0888 ± 0.0131</b>	66.63	0.494	1.336	<b>0.0897 ± 0.0115</b>	65.37	0.605	1.156
8.0	0.0516 ± 0.0001	0.00	0.258	0.487	0.0500 ± 0.0000	0.00	0.241	0.722
10.0	0.0735 ± 0.0096	77.88	0.481	1.377	0.0695 ± 0.0122	80.51	0.494	1.347

Table 20: SAC – Quadrotor3D  $w_c$  sweep ( $N_{\text{eval}} = 100$ , 2 M steps). Bold marks the best row in each section.

$w_c$	Final Model						Best-Model Checkpoint					
	MSI (s)	RTA (%)	$P_3(\varphi)$	$P_4(p)$	$P_1(p_x)$	$P_6(p_z)$	MSI (s)	RTA (%)	$P_3(\varphi)$	$P_4(p)$	$P_1(p_x)$	$P_6(p_z)$
0.25	0.0435 ± 0.0001	0.00	0.046	0.241	0.255	0.980	0.0563 ± 0.0002	0.00	0.049	0.270	0.194	0.736
1.0	0.0565 ± 0.0001	0.00	0.059	1.348	0.909	0.367	0.0584 ± 0.0001	0.00	0.034	0.458	0.149	0.245
4.0	0.0416 ± 0.0004	5.50	0.275	1.579	2.832	3.307	0.0565 ± 0.0002	0.00	0.044	0.399	2.146	1.099
8.0	0.0627 ± 0.0002	0.00	0.056	0.500	0.341	0.427	0.0856 ± 0.0005	0.00	0.111	5.280	0.347	1.083
16.0	0.0707 ± 0.0010	0.00	0.051	1.304	1.698	1.829	0.0888 ± 0.0003	0.00	0.085	6.885	1.626	0.223
24.0	0.0441 ± 0.0010	3.57	0.280	1.315	4.179	5.524	0.1342 ± 0.0004	0.00	0.036	1.410	0.660	1.473
32.0	0.0977 ± 0.0009	0.00	0.038	3.184	0.932	0.361	0.1023 ± 0.0004	0.00	0.059	4.168	0.500	1.272
40.0	0.2042 ± 0.0004	0.00	0.048	0.270	0.405	3.206	0.2019 ± 0.0004	0.00	0.051	0.275	0.376	2.687
<b>48.0</b>	<b>0.2962 ± 0.0004</b>	0.00	0.045	0.208	1.572	2.650	<b>0.3017 ± 0.0005</b>	<b>0.00</b>	0.044	0.190	1.185	4.528
56.0	<b>0.2975 ± 0.0002</b>	<b>0.00</b>	0.042	0.203	0.277	3.708	0.3008 ± 0.0004	0.00	0.043	0.195	0.361	5.289
64.0	0.2944 ± 0.0001	0.00	0.044	0.252	0.241	0.329	0.2974 ± 0.0003	0.00	0.041	0.203	0.243	1.222

**Quadrotor is robust across the tested mass range.** The Quadrotor is largely unaffected across both scaling factors (MSI within 2.5% of nominal, RTA at or below 0.2%), consistent with its 9.0° safety margin absorbing the mismatch without triggering additional interventions.

**Baseline 2 boundary case.** At 1.3× mass, the fixed-LQR controller at  $\tau_{\text{match}}$  succeeds for both Pendulum (mean episode length 50.3 s) and CartPole (50.2 s), whereas both fail at nominal mass (Table 2). The heavier plant has lower acceleration per unit input, shifting the closed-loop eigenvalues of the ZOH discretization at that fixed interval back into the stable region. This confirms that the nominal failure of B2 is a genuine dynamical instability rather than a conservative evaluation artifact, and that the RL policy’s adaptive inter-sample interval is what allows it to succeed where fixed-rate LQR cannot.

**Domain randomization.** Training with mass sampled from Uniform[0.6, 1.4]× at each episode reset substantially reduces Pendulum sensitivity: RTA activation at 0.7× mass drops from 30.48 ± 24.80% (nominal training) to 0.00% (DR), confirming that the agent has internalized faster dynamics through training diversity. For CartPole, DR reduces the 0.7× RTA activation from 13.91% to 0.16% and recovers MSI to 0.296 s, essentially matching the non-DR RL-STC (0.317 s) while eliminating mass sensitivity. For Quadrotor, already robust under nominal training, DR provides negligible additional benefit. The DR models impose minimal performance cost at the best-model checkpoint: nominal MSI values of 0.389 s, 0.319 s, and 0.290 s match the non-DR references closely. The benefit of DR scales with the magnitude of perturbation: larger mass deviations increase the one-step-ahead prediction error, causing more RTA activations and greater MSI degradation for the nominal policy; the DR policy, trained across the full deviation range, retains appropriate timing conservatism for those regimes and is correspondingly less affected.

The natural resolution to mass sensitivity would be to include plant mass in the observation, allowing the policy to condition its timing on the current dynamics. We deliberately exclude this because our goal is to evaluate a single fixed policy across mass variation, matching the deployment scenario where mass is unknown. Adding mass to the observation would require online identification of a vector quantity (for MIMO systems such as the Quadrotor, mass affects multiple actuator channels simultaneously) and constitutes a separate problem. The DR results therefore represent an inherent

Table 21: Preference-Conditioned SAC – Quadrotor3D  $w_c$  sweep ( $N_{\text{eval}} = 100$ , 4 M steps, single model, discrete sampling). Bold marks the best row in each section.

$w_c$	Final Model					Best-Model Checkpoint				
	MSI (s)	RTA (%)	$P_3(\varphi)$	$P_4(p)$	$P_1(p_x)$	MSI (s)	RTA (%)	$P_3(\varphi)$	$P_4(p)$	$P_1(p_x)$
0.25	0.064 ± 0.000	0.00	0.040	0.204	0.753	0.063 ± 0.000	0.00	0.039	0.195	0.587
1.0	0.055 ± 0.000	0.00	0.043	0.215	0.365	0.058 ± 0.000	0.00	0.042	0.201	0.347
4.0	0.071 ± 0.000	0.00	0.047	0.222	0.323	0.075 ± 0.000	0.00	0.045	0.208	1.006
8.0	0.094 ± 0.000	0.00	0.044	0.202	1.138	0.109 ± 0.000	0.00	0.047	0.224	0.557
16.0	0.178 ± 0.001	0.00	0.069	0.720	1.018	0.168 ± 0.000	0.01	0.053	0.649	2.358
24.0	0.204 ± 0.001	0.00	0.061	1.717	2.019	0.207 ± 0.001	0.00	0.066	1.316	2.317
32.0	0.202 ± 0.001	0.00	0.081	1.190	2.114	0.200 ± 0.000	0.00	0.061	0.749	2.066
40.0	0.227 ± 0.002	0.00	0.194	1.901	1.889	0.226 ± 0.000	0.00	0.173	1.513	1.031
48.0	0.240 ± 0.001	0.00	0.113	1.189	2.379	0.235 ± 0.002	0.00	0.075	0.658	1.408
56.0	0.240 ± 0.000	0.00	0.108	1.244	2.477	0.238 ± 0.002	0.00	0.060	0.617	1.904
<b>64.0</b>	<b>0.241 ± 0.000</b>	<b>0.00</b>	<b>0.100</b>	<b>1.150</b>	<b>2.464</b>	<b>0.239 ± 0.001</b>	<b>0.00</b>	<b>0.070</b>	<b>0.725</b>	<b>2.138</b>

Table 22: Quadrotor3D baselines and Ablations A & B at  $w_c = 48$  ( $N_{\text{eval}} = 100$ , best-model checkpoint). RTA % is 0 by construction for all LQR-based baselines. *Italics* = system failure (ep. length < 3 s); “–” = norms not meaningful for failed episodes.

Method	MSI (s)	RTA (%)	$P_3(\varphi)$	$P_4(p)$	$P_1(p_x)$	$P_6(p_z)$
<i>Baselines</i>						
LQR at $\tau_{\min}$ (Baseline 1)	0.040 ± 0.000	0.00	0.176	7.230	0.447	0.123
LQR at $\tau_{\text{match}} = 0.302$ s (Baseline 2)	<i>0.302</i>	<i>0.00</i>	–	–	–	–
Classical Lyapunov-STC (Baseline 3)	0.040 ± 0.000	0.00	0.176	7.235	0.444	0.118
<i>Ablation A – No RTA</i>						
No-RTA	0.310 ± 0.000	0.00	0.085	0.375	3.989	4.037
<i>Ablation B – Fixed <math>\tau</math></i>						
Fixed- $\tau$ RL ( $\tau = 0.302$ s)	0.302 ± 0.000	0.00	0.041	0.370	0.338	0.178
<i>Full Method</i>						
<b>RL-STC (SAC, <math>w_c = 48</math>)</b>	<b>0.302 ± 0.001</b>	<b>0.00</b>	<b>0.044</b>	<b>0.190</b>	1.185	4.528

robustness–performance tradeoff: meaningful sensitivity reduction for environments with genuine mass fragility (Pendulum and CartPole) at negligible cost to nominal performance.

## M.2 Disturbance Robustness: Detailed Discussion

**RL-STC dominates Classical STC even without disturbances.** The no-disturbance row of Table 27 establishes the communication-efficiency gap before any disturbance is applied: RL-STC achieves 0.389 s vs. 0.202 s for Pendulum (+93%), 0.319 s vs. 0.212 s for CartPole (+50%), and 0.290 s vs. 0.080 s for Quadrotor (+263%). Classical STC’s conservative Lyapunov trigger consistently rejects  $\tau$  values the RL policy has learned to exploit safely, fixing MSI well below the  $\tau_{\max}$  ceiling in all three environments.

**RTA acts as a graduated shield under growing disturbances.** For RL-STC, RTA activation grows monotonically with disturbance amplitude while every episode completes safely: the safety filter absorbs what the policy cannot. For the Pendulum, a constant 0.5 Nm torque (25% of  $u_{\max}$ ) drives RTA activation to 88.54% and collapses MSI to  $\tau_{\min} = 0.05$  s; at the milder 0.2 Nm level, MSI falls 36% (from 0.389 to 0.249 s) with 26% activation. CartPole is substantially more robust: even the strongest constant force tested (2.0 N, 10% of  $F_{\max}$ ) raises RTA to only  $10.11 \pm 17.22\%$  and reduces MSI by 38% (0.319 → 0.199 s). The Quadrotor shows near-complete insensitivity: MSI varies by at most 0.002 s and RTA stays within 0.81–1.13% across all conditions, because thrust disturbances perturb the altitude channel while the angular RTA trigger monitors tilt, leaving the timing policy structurally decoupled from the disturbance. Classical STC’s  $\tau$ -selection uses only the undisturbed nominal model; disturbances enter only indirectly through the next state  $\mathbf{x}_{k+1}$ . For the Pendulum this makes Cl.-STC MSI almost completely flat ( $\approx 0.200$  s) across all conditions, because disturbances are invisible to the trigger. Despite maintaining higher MSI than RL-STC under strong Pendulum disturbances, state quality is worse: under 0.5 Nm constant torque, Cl.-STC achieves  $P_3 = 0.594$  vs. RL-STC’s  $P_3 = 0.490$  (RL-STC’s 88% RTA activation imposes frequent LQR corrections that

Table 23: Lagrangian-SAC vs. RL-STC for Quadrotor3D ( $w_c = 48$ ,  $N_{\text{eval}} = 100$ ). RL-STC Hard Viol. = 0.0 by construction.

Method	Final Model			Best-Model Checkpoint		
	MSI (s)	Pred. Safety (%)	Hard Viol. (%)	MSI (s)	Pred. Safety (%)	Hard Viol. (%)
Lagrangian-SAC	$0.311 \pm 0.000$	0.01	0.00	$0.312 \pm 0.000$	0.00	0.00
<b>RL-STC</b>	<b><math>0.296 \pm 0.000</math></b>	0.00	<b>0.00</b>	<b><math>0.302 \pm 0.001</math></b>	0.00	<b>0.00</b>

Table 24: Quadrotor3D mass-mismatch robustness ( $N_{\text{eval}} = 100$ , best-model checkpoint,  $w_c = 48$ ). DR = domain-randomized training ( $\pm 40\%$  mass).

Method	Scale	MSI (s)	RTA (%)
RL-STC	$0.7\times$	$0.302 \pm 0.001$	0.00
	Nominal	$0.302 \pm 0.001$	0.00
	$1.3\times$	$0.302 \pm 0.001$	0.00
RL-STC + DR	$0.7\times$	$0.276 \pm 0.001$	0.00
	Nominal	$0.276 \pm 0.001$	0.00
	$1.3\times$	$0.276 \pm 0.001$	0.00
Classical STC	$0.7\times$	$0.040 \pm 0.000$	0.00
	Nominal	$0.040 \pm 0.000$	0.00
	$1.3\times$	$0.040 \pm 0.000$	0.00

tighten the trajectory). Under the  $0.5\text{ Nm}$   $2\text{ Hz}$  periodic case, Cl.-STC’s angular-velocity norm explodes to  $P_4 = 3.26$  vs. RL-STC’s  $P_4 = 1.36$ ; the Lyapunov trigger selects  $\tau = 0.20\text{ s}$  throughout, oblivious to the resonant forcing.

For CartPole under constant force, Cl.-STC MSI drops significantly ( $0.212 \rightarrow 0.123\text{ s}$  at  $1.0\text{ N}$ ) as the drifting cart state makes the nominal Lyapunov condition more demanding; yet despite communicating more frequently, the cart-position norm  $P_1$  worsens dramatically ( $0.065 \rightarrow 2.951\text{ m}\cdot\text{s}$ ). RL-STC simultaneously maintains higher MSI ( $0.284\text{ s}$ ) and better position tracking ( $P_1 = 3.345\text{ m}\cdot\text{s}$  with near-zero RTA activation), showing the learned policy handles constant bias more gracefully than the greedy Lyapunov trigger. For the Quadrotor, Cl.-STC is already at  $0.080\text{ s}$  in the undisturbed case; disturbances move it only slightly ( $0.080 \rightarrow 0.087\text{ s}$ ), mirroring the structural insensitivity of RL-STC but at a communication cost  $3.6\times$  higher.

**Impulse disturbances reveal bimodal RL-STC behavior.** Random impulse kicks ( $p = 0.05$  per RL step) produce strikingly different responses. The Pendulum is highly sensitive: a  $0.5\text{ Nm}$  kick collapses RL-STC MSI to  $0.252 \pm 0.063\text{ s}$  and raises RTA activation to  $38.38 \pm 18.59\%$ . The large standard deviation reflects bimodal episode behavior: some episodes receive well-timed kicks that sustain RTA engagement, while others see none. CartPole and Quadrotor are resilient: the largest impulses produce  $\leq 1\%$  RTA activation and  $\leq 2\%$  MSI change, for the same structural reasons described above (angular RTA trigger is decoupled from the thrust/force disturbance channel for the Quadrotor). Classical STC is insensitive to impulses in all environments, since a rare kick shifts the state only marginally relative to the Lyapunov basin.

Table 25: Quadrotor3D disturbance robustness ( $N_{\text{eval}} = 100$ , best-model checkpoint,  $w_c = 48$ ). Disturbance applied as additive thrust deviation ( $\delta F$ , N).

Condition	RL-STC MSI (s)	Cl.-STC MSI (s)	RTA (%)
No disturbance	$0.302 \pm 0.001$	$0.040 \pm 0.000$	0.00
<i>Constant</i>			
0.5 N	$0.302 \pm 0.001$	$0.040 \pm 0.000$	0.00
1.0 N	$0.302 \pm 0.001$	$0.040 \pm 0.000$	0.00
<i>Periodic</i>			
0.8 N, 1 Hz	$0.302 \pm 0.001$	$0.040 \pm 0.000$	0.00
1.5 N, 2 Hz	$0.301 \pm 0.001$	$0.040 \pm 0.000$	0.00
<i>Impulse (<math>p = 0.05</math>, random sign)</i>			
1.0 N	$0.302 \pm 0.001$	$0.040 \pm 0.000$	0.00
2.0 N	$0.302 \pm 0.001$	$0.040 \pm 0.000$	0.00

Table 26: Model-mismatch robustness: mass scaled to  $0.7\times$  and  $1.3\times$  nominal ( $N_{\text{eval}} = 100$ , seed 0 for RL-STC and RL-STC+DR). DR = domain randomization (mass from Uniform $[0.6, 1.4] \times$  nominal at each episode reset;  $K$ ,  $P$ , and RTA thresholds fixed at nominal). Best-model checkpoint reported for all variants. *Italics* = system failure (mean episode length  $< 5$  s); “-” = RTA not applicable.

Method	Scale	Pendulum		CartPole		Quadrotor	
		MSI (s)	RTA (%)	MSI (s)	RTA (%)	MSI (s)	RTA (%)
RL-STC	$0.7\times$	$0.246 \pm 0.078$	$30.48 \pm 24.80$	$0.201 \pm 0.025$	$13.91 \pm 6.09$	$0.284 \pm 0.008$	$0.15 \pm 0.31$
RL-STC	Nominal	$0.396 \pm 0.001$	0.00	$0.317 \pm 0.001$	0.00	$0.290 \pm 0.005$	$0.17 \pm 0.33$
RL-STC	$1.3\times$	$0.349 \pm 0.007$	$4.99 \pm 1.68$	$0.309 \pm 0.006$	$0.81 \pm 1.47$	$0.291 \pm 0.005$	$0.14 \pm 0.28$
RL-STC+DR	$0.7\times$	$0.383 \pm 0.004$	0.00	$0.296 \pm 0.010$	$0.16 \pm 0.70$	$0.286 \pm 0.005$	$1.23 \pm 0.87$
RL-STC+DR	Nominal	$0.389 \pm 0.003$	$0.04 \pm 0.25$	$0.319 \pm 0.002$	$0.02 \pm 0.12$	$0.290 \pm 0.005$	$1.03 \pm 0.84$
RL-STC+DR	$1.3\times$	$0.344 \pm 0.041$	$6.42 \pm 13.03$	$0.315 \pm 0.005$	$0.29 \pm 0.79$	$0.292 \pm 0.005$	$0.88 \pm 0.81$
Cl.-STC	$0.7\times$	<i><math>0.092 \pm 0.011</math></i>	-	<i><math>0.176 \pm 0.012</math></i>	-	$0.080 \pm 0.000$	-
Cl.-STC	Nominal	$0.202 \pm 0.000$	-	$0.212 \pm 0.001$	-	$0.080 \pm 0.001$	-
Cl.-STC	$1.3\times$	$0.328 \pm 0.003$	-	$0.266 \pm 0.001$	-	$0.080 \pm 0.000$	-

Table 27: Disturbance robustness: RL-STC MSI, Classical STC MSI, and RTA activation under constant, periodic, and impulse disturbances ( $N_{\text{eval}} = 100$ , best-model checkpoint, seed 0 for RL-STC,  $w_c = 8/16/16$ ).  $K$ ,  $P$ , and RTA thresholds fixed at nominal. Pendulum: torque ( $u_{\text{max}} = 2$  Nm); CartPole: force ( $F_{\text{max}} = 20$  N); Quadrotor: thrust deviation ( $\delta F_{\text{max}} = 5$  N). Impulse per RL step ( $p = 0.05$ , random sign).

Condition	Pendulum			CartPole			Quadrotor		
	RL-STC	Cl.-STC	RTA (%)	RL-STC	Cl.-STC	RTA (%)	RL-STC	Cl.-STC	RTA (%)
	MSI (s)			MSI (s)			MSI (s)		
None	$0.389 \pm 0.003$	0.202	$0.04 \pm 0.25$	$0.319 \pm 0.002$	0.212	$0.02 \pm 0.12$	$0.290 \pm 0.005$	0.080	$1.03 \pm 0.84$
Const. 0.2 Nm / 1.0 N / 0.5 N	$0.249 \pm 0.036$	0.200	$26.45 \pm 12.90$	$0.284 \pm 0.025$	0.123	$0.75 \pm 1.89$	$0.291 \pm 0.005$	0.082	$0.81 \pm 0.66$
Const. 0.5 Nm / 2.0 N / 1.0 N	$0.079 \pm 0.011$	0.199	$88.54 \pm 7.18$	$0.199 \pm 0.065$	0.121	$10.11 \pm 17.22$	$0.289 \pm 0.005$	0.082	$1.12 \pm 0.74$
Per. 0.3 Nm 1 Hz / 1.5 N / 0.8 N	$0.333 \pm 0.013$	0.200	$5.11 \pm 3.53$	$0.270 \pm 0.028$	0.188	$2.38 \pm 5.12$	$0.290 \pm 0.005$	0.083	$1.13 \pm 0.77$
Per. 0.5 Nm 2 Hz / 2.5 N / 1.5 N	$0.108 \pm 0.024$	0.200	$77.21 \pm 10.70$	$0.250 \pm 0.037$	0.174	$5.42 \pm 9.68$	$0.289 \pm 0.005$	0.086	$0.98 \pm 0.77$
Imp. 0.5 Nm / 2.0 N / 1.0 N	$0.252 \pm 0.063$	0.200	$38.38 \pm 18.59$	$0.305 \pm 0.017$	0.200	$0.90 \pm 3.22$	$0.289 \pm 0.005$	0.087	$1.10 \pm 0.83$
Imp. 1.0 Nm / 4.0 N / 2.0 N	$0.242 \pm 0.075$	0.199	$41.95 \pm 21.31$	$0.311 \pm 0.015$	0.204	$0.00 \pm 0.00$	$0.290 \pm 0.005$	0.087	$1.01 \pm 0.86$

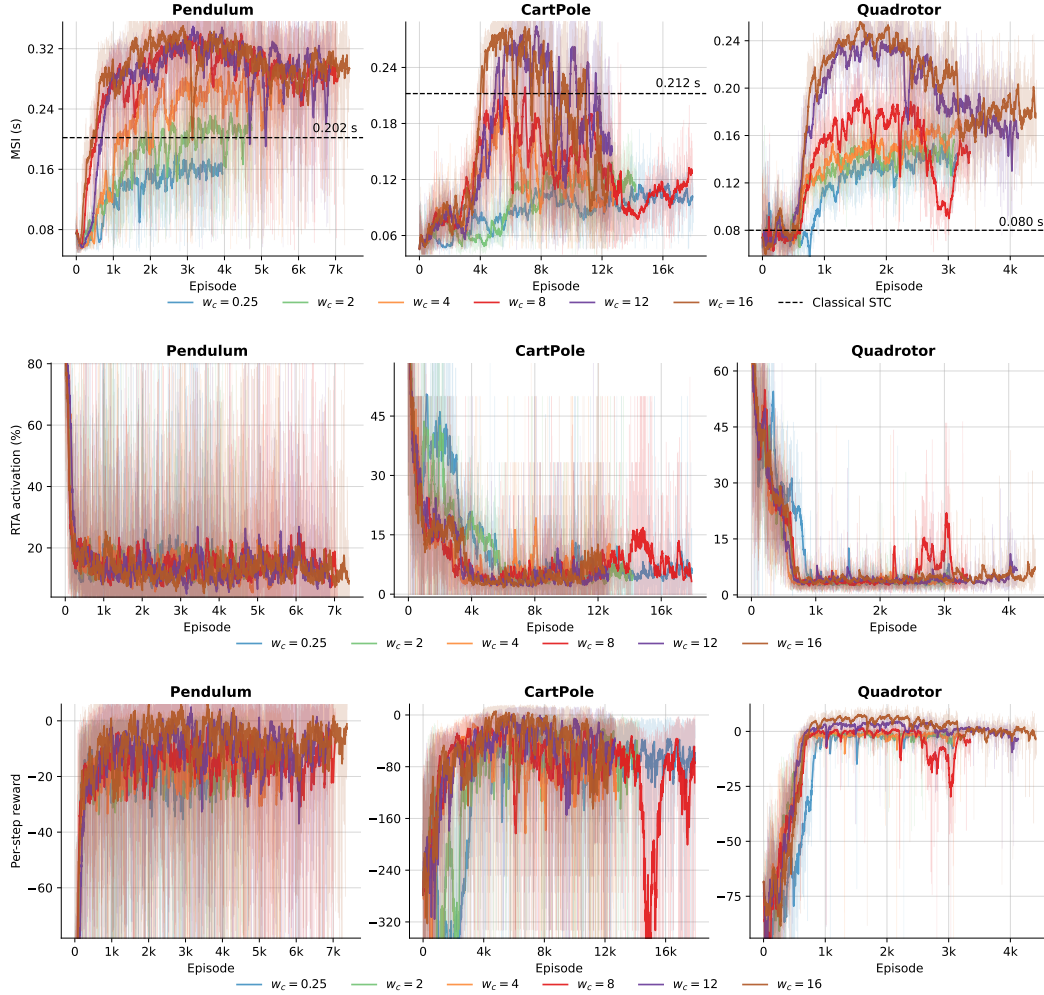


Figure 4: DQN training curves for five  $w_c$  values across the three lower-dimensional environments (seed-0 runs from the multi-seed sweep). **(top)** Mean inter-sample interval; dashed line shows the Classical STC baseline. **(middle)** RTA activation rate (%). **(bottom)** Per-step reward. Faint traces are raw per-episode data; bold lines are EMA-smoothed ( $\alpha = 0.06$ ,  $\approx 17$ -episode window). Higher  $w_c$  accelerates exploration of the sparse-sampling regime; the MSI peak before reward collapse motivates the best-model checkpoint strategy.

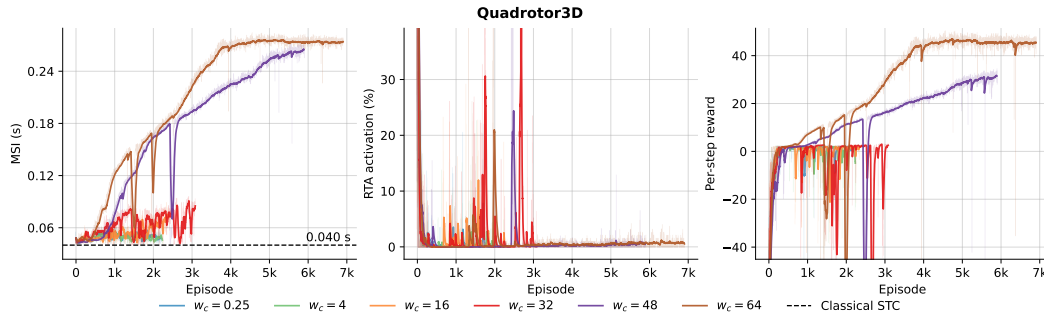
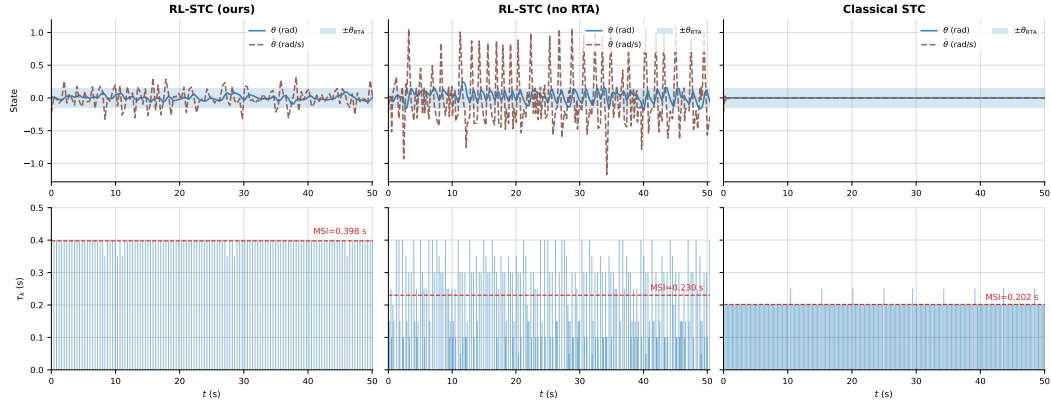
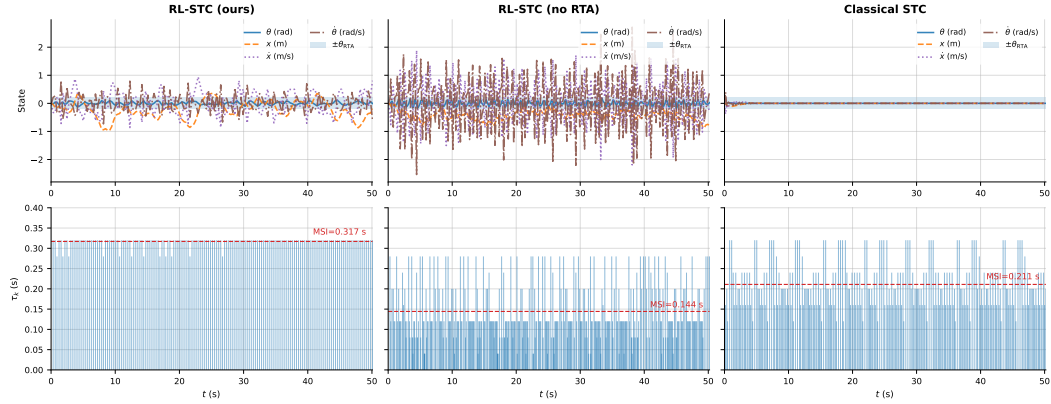


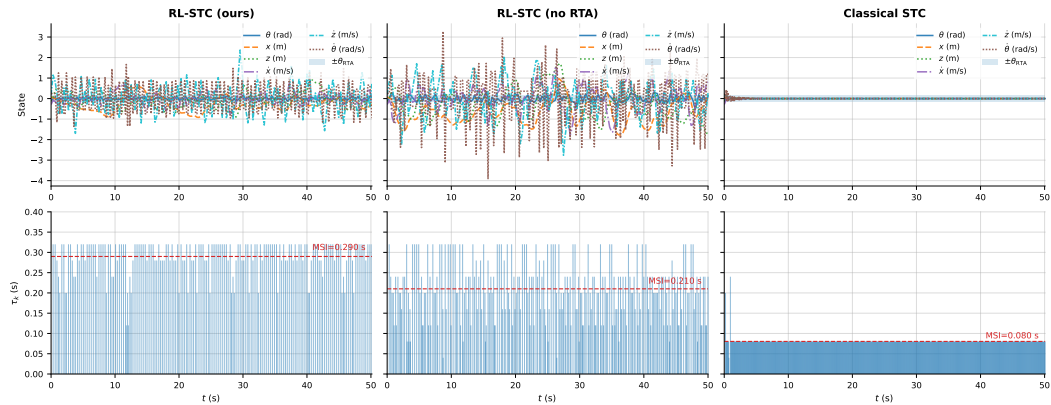
Figure 5: SAC training curves for six representative  $w_c$  values on Quadrotor3D (2 M steps, seed 0). **(left)** Mean inter-sample interval; dashed line shows Classical STC pinned at  $\tau_{\min}$ . **(center)** RTA activation rate (%). **(right)** Per-step reward. Faint traces are raw per-episode data; bold lines are EMA-smoothed ( $\alpha = 0.06$ ,  $\approx 17$ -episode window). The two-phase dynamic from Section 6 is visible:  $w_c \leq 16$  keeps MSI near  $\tau_{\min}$  during training, while  $w_c \geq 40$  saturates near  $\tau_{\max}$  at 0% RTA.



(a) Pendulum



(b) CartPole



(c) Quadrotor

Figure 6: Representative episode trajectories on the three lower-dimensional environments (seed 0, up to 1200 steps). Each sub-figure: **left** RL-STC (ours); **center** RL-STC without RTA (Ablation A); **right** Classical Lyapunov-STC. Top row: state trajectories with  $\pm\theta_{RTA}$  band. Bottom row: inter-sample intervals  $\tau_k$ ; red stems = RTA-active steps; dashed line = MSI. The Quadrotor sub-figure highlights the dramatic MSI gap: the RL policy sustains long inter-sample intervals near hover while the classical trigger remains near  $\tau_{min}$  throughout.